Manuscript
Click here to download Manuscript: Garcia-Diaz et al.BSF.doc
Click here to view linked References

*Title:* **Loss of lysophosphatidic acid receptor $LPA_1$ alters oligodendrocyte differentiation and myelination in the mouse cerebral cortex.**

*Author names:* Beatriz García-Díaz (1,2), Raquel Riquelme (3), Isabel Varela-Nieto (3), Antonio Jesús Jiménez (4), Isabel de Diego (5), Ana lsabel Gómez-Conde (6), Elisa Matas-Rico (1,7), José Ángel Aguirre (8), Jerold Chun (9), Carmen Pedraza (10), Luis Javier Santín (10), Oscar Fernández (11), Fernando Rodríguez de Fonseca (12), Guillermo Estivill-Torrús (1,6).

*Author affiliations:*

(1) Laboratorio de Investigación, UGC Intercentros de Neurociencias, Instituto de Investigación Biomédica de Málaga (IBIMA), Hospitales Universitarios Regional de Málaga y Virgen de la Victoria, E-29010, Málaga, Spain.

(2) Department of Neurology, H. Houston Merritt Clinical Research Center, Columbia University Medical Center, New York, NY 10032, USA.

(3) Instituto de Investigaciones Biomédicas 'Alberto Sols', Consejo Superior de Investigaciones Científicas (CSIC), Universidad Autónoma de Madrid (UAM), E-28029 Madrid, Spain.

(4) Departamento de Biología Celular, Genética y Fisiología, Instituto de Investigación Biomédica de Málaga (IBIMA), Universidad de Málaga, E-29071 Málaga, Spain.

(5) Departamento de Anatomía y Medicina Legal, Universidad de Málaga, E-29071, Málaga, Spain.

(6) ECAI de Microscopía, Instituto de Investigación Biomédica de Málaga (IBIMA), Hospitales Universitarios Regional de Málaga y Virgen de la Victoria, E-29010, Málaga, Spain.

(7) Division of Cell Biology I, The Netherlands Cancer Institute, Amsterdam, 1066CX, The Netherlands.

(8) Departamento de Fisiología Humana y Educación Físico Deportiva, Universidad de Málaga, E-29071, Málaga, Spain.

(9) Department of Molecular and Cellular Neuroscience, Dorris Neuroscience Centre, The Scripps Research Institute, La Jolla, CA, 92037, USA.

(10) Departamento de Psicobiología y Metodología de las Ciencias del Comportamiento. Instituto de Investigación Biomédica de Málaga (IBIMA), Universidad de Málaga, E-29071 Málaga, Spain.

(11) Neurology Service, UGC Intercentros de Neurociencias, Instituto de Investigación Biomédica de Málaga (IBIMA), Hospitales Universitarios Regional de Málaga y Virgen de la Victoria, Universidad de Málaga, E-29010, Málaga, Spain.

(12) Laboratorio de Medicina Regenerativa, UGC de Salud Mental, Instituto de Investigación Biomédica de Málaga (IBIMA), Hospital Universitario Regional de Málaga, E-29010 Málaga, Spain.

*Correspondence should be addressed to*: Guillermo Estivill-Torrús; Laboratorio de Investigación, UGC Intercentros de Neurociencias, Instituto de Investigación Biomédica de Málaga (IBIMA), Hospitales Universitarios Regional de Málaga y Virgen de la Victoria, Hospital Civil, Pabellón 5, planta sótano, Plaza del Hospital Civil s/n, E-29009, Málaga, Spain; tel: + 34 951290346. e-mail: guillermo.estivill@ibima.eu

*Keywords:* lysophosphatidic acid receptor; myelin; oligodendrocyte; cerebral cortex.

**Abstract**

Lysophosphatidic acid (LPA) is an intercellular signaling lipid that regulates multiple cellular functions, acting through specific G-protein coupled receptors ($LPA_{1-6}$). Our previous studies using viable *Malaga* variant ma$LPA_1$-null mice demonstrated the requirement of the $LPA_1$ receptor for normal proliferation, differentiation and survival of the neuronal precursors. In the cerebral cortex $LPA_1$ is expressed extensively in differentiating oligodendrocytes, in parallel with myelination. Although exogenous LPA-induced effects have been investigated in myelinating cells, the in vivo contribution of $LPA_1$ to normal myelination remains to be demonstrated. This study identified a relevant in vivo role for $LPA_1$ as a regulator of cortical myelination. Immunochemical analysis in adult ma$LPA_1$-null mice demonstrated a reduction in the steady-state levels of the myelin proteins MBP, PLP/DM20 and CNPase in the cerebral cortex. The myelin defects were confirmed using magnetic resonance spectroscopy and electron microscopy. Stereological analysis limited the defects to adult differentiating oligodendrocytes, without variation in the $NG2^+$ precursor cells. Finally, a possible mechanism involving oligodendrocyte survival was demonstrated by the impaired intracellular transport of the PLP/DM20 myelin protein which was accompanied by cellular loss, suggesting stress-induced apoptosis. These findings describe a previously uncharacterized in vivo functional role for $LPA_1$ in the regulation of oligodendrocyte differentiation and myelination in the CNS, underlining the importance of the ma$LPA_1$-null mouse as a model for the study of demyelinating diseases.

## Introduction

Lysophosphatidic acid (LPA) is a simple phospholipid with important biological functions that acts through specific G protein-coupled receptors ($LPA_{1-6}$) as an intercellular mediator in cellular responses involving proliferation, differentiation, survival and cell migration (Anliker and Chun 2004; Moolenaar et al. 2004; Birgbauer and Chun 2006; Noguchi et al. 2009; Choi et al. 2010; Choi and Chun 2013). Bioactive lysophospholipids and their receptors have been proposed as new targets in lipidomic-based therapeutics for neuroimmunological diseases (Brinkmann and Lynch 2002; Chun 2005; Chun and Rosen 2006; Lin et al. 2010; Tigyi, 2010; Choi and Chun 2013), and many of these diseases are frequently accompanied by myelin disruption-associated symptoms, such as neuropathic pain, multiple sclerosis, or demyelinating neuropathies. The identification of novel signaling mechanisms in these conditions might enable the development of therapies aimed at facilitating spontaneous remyelination and subsequent functional recovery.

Peripherally, a recent study has showed the involvement of the $LPA_1$ receptor in Schwann cell migration and nerve development, including myelination, in sciatic nerves (Anliker et al. 2013). Notwithstanding these studies, the function of $LPA_1$ receptor in brain myelination remains to be demonstrated. A role in the regulation of cortical myelination has been suggested for the $LPA_1$ receptor because of its expression in postnatal mature oligodendrocytes in association with the onset of myelination in the brain (Allard et al. 1998; Weiner et al. 1998; Möller et al. 1999; Handford et al. 2001; Cervera et al. 2002; Yu et al. 2004). The pharmacological response to LPA is apparently restricted to newly differentiated nonmyelinating and differentiating oligodendrocytes, affecting the formation of processes (Möller et al. 1999; Dawson et al. 2003) and the later stages of maturation (Matsushita et al. 2005; Nogaroli et al. 2009), but not the genuine precursors or mature oligodendrocytes (Stankoff et al. 2002). It is precisely during this

period that differentiating cortical oligodendrocytes exhibit activity of secreted endogenous autotaxin, the enzyme that generates extracellular LPA (Fox et al. 2003; Dennis et al. 2008; Nogaroli et al. 2009). However, in addition to the responsiveness of exogenous LPA, further studies will be needed to demonstrate the in vivo function of LPA in the cortical myelination.

To gain new insights into the bona fide role of the $LPA_1$ receptor in myelination in vivo, in this study we analyzed a mouse model carrying a mutation in the *Lpar1* gene. The maLPA$_1$-null mouse, or "Malaga variant" (Estivill-Torrús et al. 2008), is a stable variant of the original LPA$_1$-null mutant (Contos et al. 2000) that carries the deletion of exon 3, which contains the transmembrane domains I–VI of the receptor. This variant exhibits more pronounced defects than the original mutant, including defects affecting the development of cortical precursors (Estivill-Torrús et al. 2008), adult hippocampal neurogenesis (Matas-Rico et al. 2008), and motor, emotional and cognitive alterations involving long-term spatial, contextual and episodic-like memory (Santín et al. 2009; Castilla-Ortega et al. 2010, 2011, 2012; Blanco et al. 2012; García-Fernández et al., 2012; Estivill-Torrús et al. 2013; Pedraza et al., 2013).

In this study, we report that the mice lacking the $LPA_1$ receptor exhibited a reduction in cortical oligodendrocytes and defective myelination, affecting the cortical steady-state levels of myelin proteins and eventually the quantity, quality and organization of the myelinated fibers. These aspects made the maLPA$_1$-null mouse an interesting experimental model for the study of diseases affecting cortical myelination. Interestingly, the absence of the $LPA_1$ receptor resulted in the accretion of the myelin proteolipid protein (PLP) in the endoplasmic reticulum and correlated with cellular loss, suggesting stress-induced apoptosis. Our findings demonstrate for the first time a functional in vivo role for the LPA$_1$-mediated pathway in normal cortical myelination.

## Materials and Methods

*Animals*. The mice were generated and characterized as described previously (Estivill-Torrús et al. 2008; Matas-Rico et al. 2008). The maLPA$_1$-null mouse (or *Málaga* variant; Estivill-Torrús et al. 2008) was derived spontaneously from the original LPA$_1$-null mouse (Contos et al. 2000) during colony expansion by crossing heterozygous foundational parents (maintained in the original hybrid C57BL/6J × 129X1/SvJ background). The descendants were backcrossed within the same background and for more than twenty generations, the progeny were born at the expected Mendelian ratio. Similar to the original null mice, maLPA$_1$-null mice maintained the targeted gene disruption of the *Lpar1* gene exon 3 codifying domains I and VI in the LPA$_1$ receptor (Contos et al. 2000) as demonstrated through genotyping (according Contos et al. 2000) and immunohistochemistry (Estivill-Torrús et al. 2008).

This study was performed on young (postnatal day 10 to P30) and 3-month-old male mice, wild-type [ma*Lpar1*$^{(+/+)}$, also termed normal in this work] and maLPA$_1$-null homozygotes [ma*Lpar1*$^{(-/-)}$, termed null or maLPA$_1$-null (Estivill-Torrús et al. 2008)]. Animals were housed under standard conditions of temperature, air, humidity, lighting and water and food supply. The experiments were performed in compliance with European animal research laws (European Communities Council Directives 2010/63/UE, 90/219/CEE, Regulation (EC)nº1946/2003) and Spanish National and Regional Guidelines for Animal Experimentation and Use of Genetically Modified Organisms (Real Decreto 53/2013, Ley 32/2007 and Ley 9/2003, Real Decreto 178/2004, Decreto 320/2010).

*Immunohistochemistry and stereological analysis.* To investigate the effects of the absence of LPA$_1$ on myelination 50 µm brain coronal sections were immunolabeled overnight with a series of antibodies against the following antigens: 2', 3'-cyclic nucleotide 3'-phosphodiesterase (CNPase)

(1:500; mouse monoclonal; Sigma-Aldrich Co., St. Louis, MO), galactocerebroside (GalC) (1:500; mouse monoclonal; EMD Millipore Corporation, Billerica, MA), glial fibrillary acidic protein (GFAP) (1:1000; rabbit polyclonal; DakoCytomation, Glostrup, Denmark), Golgi phosphoprotein 4 (Golph4) (1:400; rabbit polyclonal; Abcam Plc., Cambridge, UK), lysosome associated membrane protein (LAMP1) (1:400; rabbit polyclonal; Abcam), lysophosphatidic acid receptor 1 ($LPA_1$) (1:200; rabbit polyclona; Thermo Fisher Scientific Inc., Rockford, IL; see online resource), 200 kD neurofilament H (1:1000; rabbit polyclonal antibody; Sigma; see online resource), myelin basic protein (MBP) (1:200/1:1000; rat/rabbit polyclonal; Abcam/Millipore), myelin/oligodendrocyte-specific protein (MOSP) (1:500; mouse monoclonal; Millipore), chondroitin sulfate proteoglycan (NG2) (1:500; rabbit polyclonal; Millipore), oligodendrocyte lineage transcription factor 2 (Olig2) (1:750; rabbit polyclonal; Millipore), protein disulphide isomerase (PDI) (1:100; rabbit polyclonal; Abcam), and proteolipid protein (PLP and DM20) (1:100; mouse monoclonal; Millipore). For the detection step, biotin conjugated rabbit anti-mouse, swine anti-rabbit immunoglobulins (DakoCytomation), goat anti-rat IgG (Serotec) (as appropriate), ExtrAvidin®-peroxidase (Sigma) and DAB (Sigma) were used. The antibodies were diluted in blocking solution [PBS containing 0.5% Triton X-100 and 2.5% normal serum (rabbit or swine serum, depending of the source of the secondary reagent used)]. Omission of the primary antibody resulted in no detectable staining. All steps were carried out at room temperature (~20ºC).

In all procedures, at least eight animals were used for each experimental condition and per genotype. Adult 3-month-old and young (postnatal day 10 to P30) male mice were deeply anesthetized with ketamine and xylazine (400 and 60 mg/kg, respectively, ip.) and were transcardially perfused with saline solution, followed by 20–30 min fixation using, in the majority of cases, 4% paraformaldehyde/ PBS containing 0.08% glutaraldehyde and 15% (v/v) saturated

picric acid (Somogyi and Takagi 1982). Specifically, fixation with 4% paraformaldehyde/ PBS was used for NG2 detection, 4% paraformaldehyde/ PBS containing 0.25% glutaraldehyde was used for CNPase detection, and 4% paraformaldehyde/PB containing 0.075 M lysine, and 0.01 M sodium periodate (Mclean and Nakane 1974), for $LPA_1$ detection. The brains were dissected out and postfixed overnight at 4°C. The majority of the immunohistochemical techniques were performed on free-floating 50 µm (10 µm for the analysis of cell morphology) vibratome sections after the samples were embedded in agar. $LPA_1$ detection was performed on free-floating 50 µm cryosections obtained using a freezing microtome. For this purpose, the tissue was cryoprotected in 30% (w/v) sucrose after fixation.

For double labeling, confocal analysis was used in conjunction with double light microscopy. Accordingly, the secondary antibodies used for immunofluorescence were goat Alexafluor® 555 anti-mouse IgG, Alexafluor® 568 anti-rat IgG, or Alexafluor® 488 anti-rabbit IgG antibodies (1:5000; Invitrogen) depending on the primary antibody used. After washing, the slides were coverslipped with Fluoromount ™ (Sigma-Aldrich) before viewing on a Leica laser TCS NT confocal fluorescence microscope. All analyses were done in sequential scanning mode in order to rule out cross-bleeding between detection channels. The cells were considered double-labeled if both fluorophores were seen within the same cell in three consecutive 1 µm optical sections in the z axis. The images were processed using Adobe Photoshop 7.0 (Adobe Systems Inc., San Joe, CA). An additional analysis was performed using double immunohistochemistry under conventional fluorescence or light microscopy using DAB and alkaline phosphatase. In this case, after visualization using DAB, slices were washed and processed for the second staining at room temperature. Accordingly, the slices were first washed thoroughly in Tris-buffered saline (TBS) containing 0.05 M Tris-HCl and 0.15 M NaCl, pH 7.5, and were subsequently incubated in the antibody solution overnight. Secondary detection was performed using the corresponding alkaline

phosphatase-conjugated antibody and an NBT/BCIP solution (Roche Diagnostics Co., Indianapolis, IN) containing 18.75 mg/ml NBT (nitro blue tetrazolium chloride) and 9.4 mg/ml BCIP (5-bromo-4-chloro-3-indolyl phosphate, toluidine salt) in 67% DMSO (v/v). The results were analyzed using an Olympus BX51 microscope equipped with an Olympus DP70 digital camera (Olympus Co., Shinjuku, Tokyo, Japan)

For the stereological analysis, a sampling of cells on the vibratome sections was analyzed throughout the motor cortex in the rostrocaudal dimension using both the optical dissector method (West et al. 1993; Gundersen et al. 1998) and the optical fractionator method, which combines the optical dissector with a fractionator sampling scheme (Gundersen et al. 1988) to exclude volume divergences. The motor cortex was delineated in accordance with the stereotaxic coordinates (described in Paxinos and Franklin 2001), from 2.46 mm to -1.34 mm, using a 10x objective lens. C.A.S.T. Grid software (Olympus) was used with a 100x objective to generate randomly sampling frames where the stained oligodendrocytes were present. For the optical dissector quantification, immunoreactive cells were counted in 12 representative 50 µm evenly spaced sections per animal. Two series per animal and six animals per genotype were analyzed. A random set of sampling optical dissectors was generated for each section, and 50% of the total sampling optical dissectors were measured. Each optical dissector consisted of a 43.4 µm × 43.4 µm sampling frame, including the exclusion lines. The starting point for counting was set at 5 µm below the surface and focused labeled cells through the 15 µm section optical plane were considered. The number of cells per unit of volume (*N*v) was calculated for each animal, as the number of applied dissectors multiplied by Vdis; Vdis = Sd x Hd, where Sd = area of the dissector grid (counting frame) and Hd = depth of dissector. When the fractionator method was used, the sections were sampled every 200 µm. A random set of sampling frames with a known area ($a_{frame}$) was generated for each section using the C.A.S.T. Grid. After counting the objects ($\Sigma Q^-$), the total number of positive

cells was estimated as follows: $N = \Sigma Q^- \times 1/ssf \times 1/asf \times 1/tsf$ (Gundersen et al. 1988), where *ssf* is the numerical fraction of the section used or the section sampling fraction, *asf* is the area sampling fraction and *tsf* is the thickness sampling fraction. The coefficient of error (CE) for each estimation and animal ranged from 0.05 to 0.1. Data were tested for significant differences between groups by ANOVA or Kruskal-Wallis one-way analysis of variance. The statistical analyses were performed on at least six animals per group, using Sigma Stat 3.0 and Sigma plot 8.0 software (Systat Software Inc., Chicago, IL). Values of $p < 0.05$ were considered significant.

*Apoptosis.* Eight adult animals per genotype were anesthetized as described above and perfused transcardially using a 4% paraformaldehyde/PBS solution. The brains were dissected out, fixed overnight in the same solution at 4ºC and processed for paraffin embedding and sectioning (10 µm). Coronal sections were obtained and mounted onto poly-L-lysine-treated slides. Cell death was detected using terminal UTP nick end labeling (TUNEL)-based procedures i.e., using the In Situ Cell Death Detection Kit, AP (Roche Diagnostics) and NeuroTACS-II™ (Trevigen Inc., Gaithersburg, MD) for wax and vibratome sections, respectively, in accordance with the manufacturer's instructions. Pretreatment of sections with DNAse I or TACS-nuclease™ served as a positive control for the enzymatic procedures; omission of the enzyme served as a negative control. Non-adjacent coronal sections were counterstained and cell numbers were estimated. For the stereological analysis of cortical apoptosis, *N*v was calculated as previously mentioned. In addition, the apoptotic cells in the corpus callosum were estimated using the Image J 1.46k software (http://imagej.nih.gov/ij/, National Institutes of Health NIH, Bethesda, MD). For each section, the number of labelled cells was estimated in a 200 µm x 200 µm counting frame positioned within the corpus callosum area. The statistical analyses were performed using the t-

student test with at least six animals per group using Sigma Stat 3.0 and Sigma plot 8.0 software. Values of $p < 0.05$ were considered significant.

*Myelin isolation, SDS-PAGE and Western blotting.* Brain protein lysates were obtained from adult mice (eight per genotype). The animals were killed by cervical dislocation and the brain was removed and stored at -80ºC until dissection. The cerebral cortices were dissected on ice, under binocular microscope, detached from the corpus callosum and anatomically separated in superficial (I to III) and deep (IV to V) layers at the level of layer IV. Layer VI was excluded to avoid contamination of the sampling with the corpus callosum. The myelin was purified by sucrose gradient centrifugation (Norton and Poduslo 1973). Accordingly, the cortex samples were homogenized (on ice) in 0.35 M sucrose and 5 mM EGTA. The suspension was overlaid onto an equivalent volume of 0.85 M sucrose and 5 mM EGTA and centrifuged at 10,000 x g at 4ºC for 20 min. The myelin-containing material at the interface was collected, diluted threefold in distilled water and centrifuged at 10,000 x g at 4ºC for 30 min. After washing the pellet with distilled water, the isolated myelin was resuspended in 20 mM Tris-HCl, aliquoted, and stored at –20ºC.

Extracts containing equal amounts of protein (5 µg) were solubilized in SDS reducing sample preparation buffer, loaded onto 15% polyacrylamide gels, and electrophoresed at 200 V constant voltage using a Mini-PROTEAN® 3 Cell system (Bio-Rad Laboratories, Inc., Hercules, CA) in accordance with the manufacturer's instructions. The Mini Trans-Blot® Electrophoretic Transfer Cell (Bio-Rad) was used to transfer the separated proteins onto PVDF membranes. The transfer was performed overnight at 4ºC at 50 V constant voltage. The membranes were blocked for 1h in PBS containing 2.5% bovine serum albumin (pH 7.4), washed in PBST (PBS with 0.2% Tween® 20, Sigma-Aldrich), and incubated overnight in the primary antibodies described previously: anti-CNPase (1:2300), anti-MBP (1:7000) ,and anti-PLP/DM20 (1:7:000), diluted in PBST. A mouse

monoclonal anti-GAPDH antibody (Santa Cruz Biotechnology, Inc., Paso Robles, CA) was used as the sampling control (1:500, diluted in PBST). The next day, the membranes were washed in PBST, incubated in the appropriate biotinylated secondary antibody for 2 h, washed and exposed to Extravidin® (Sigma-Aldrich) (1:2000 in PBST) for 1h in dark. The bands were developed using 4-chloro-1-naphthol (Opti4CN™, Bio-Rad) in accordance with the manufacturer protocol. The membrane incubations and the developing reactions were performed at room temperature. The reaction was stopped using distilled water, and the membranes were allowed to air-dry. The expression of each protein was quantified by densitometry using the OptiQuant v.4.00 software program (Packard Instruments-Co., Meriden, CT). For each antibody, the protein extracts from both genotypes were compared simultaneously in the same membrane. The statistical analyses to compare the average expression between groups were performed using the t-student test and the Sigma Stat 3.0 and Sigma Plot 8.0 software. Values of $p < 0.05$ were considered significant.

*Magnetic resonance imaging and spectroscopy.* The experiments were performed on mice at different ages, ranging from P30 up to P140, using at least four mice per age and genotype. Spontaneously breathing mice were anesthetized in an induction box by inhalation of oxygen (1 l/min) containing 3% of isofluorane, and were maintained under anesthesia during the experiment by the administration of 1-2% o isofluorane in $O_2$. During the measurement procedure, the animals were placed in a heated probe, which maintained the core body temperature at approximately 37ºC. The physiological state of the animals was monitored using a Bio Trig physiological monitor (Bruker BioSpin Co., The Woodlands, TX) to measure the respiratory rate and body temperature, which allowed the adjustment of the anesthetic concentration. 1H magnetic resonance spectroscopy and imaging experiments were performed on a Bruker Pharmascan system (Bruker BioSpin) using a 7.0-T horizontal-bore superconducting magnet equipped with a 23 mm

1H selective birdcage resonator and a 90-mm diameter Bruker gradient insert (maximum intensity 300 mT/m). The magnet was interfaced to a Hewlett-Packard console running Paravision software (Bruker BioSpin) operating on a Linux platform. T2-weighted (T2-W) spin-echo anatomical images were acquired using a rapid acquisition with relaxation enhancement (RARE) sequence in sagittal orientation, using the following parameters: TR (repetition time) = 2,500 ms, TE (echo time) = 60 ms, RARE factor = 8, Av = 3, FOV = 2.3 x 2.3 cm, acquisition matrix = 256 x 256, corresponding to an in-plane resolution of 90 μm x 90 μm and a slice thickness of 1.00 mm, achieved by acquiring 10 slices. The in vivo spectroscopy protocol used was PRESS (point-resolved spatially spectroscopy) combined with VAPOR (variable power pulses with optimized relaxation delays) water suppression (Penet et al. 2006). The spectra were acquired from a voxel in the central mouse brain, containing the thalamus and surrounding areas. The parameters used were as follows: TR = 3,000 ms, TE = 35 ms, Av = 128, and volume = 3 $mm^3$. The metabolite concentrations were determined for N-acetylaspartate (NAA), creatine (Cr) and choline (Ch); the in vivo values were obtained for the main resonances of NAA at 2.01 ppm, Cr at 3.02 ppm, and Ch at 3.21 ppm. The peak areas were calculated using the MestRe-C software (University of Santiago de Compostela, La Coruña, Spain), and the area ratios were obtained and statistical analysis was performed using these values.

*Electron microscopy*. For the ultrastructural analysis, 3-month-old mice were anesthetized by intraperitoneal administration of sodium pentobarbital (0.2 mg/g; Dolethal®, Vétoquinol E.V.S.A., Alcobendas, Madrid, Spain) and perfused transcardially with a solution consisting of 2% paraformaldehyde and 2.5% glutaraldehyde in 0.1 M phosphate buffer, pH 7.4. The brains were dissected out and postfixed overnight in the same solution. Slices of the brain cortex, 1 to 2 mm thick, were postfixed in 1% osmium tetroxide for 1 h at 4ºC and embedded in araldite epoxy

resin for polymerization for up to 48 h at 60ºC. The semithin sections, 1 µm thick, were stained with 1% toluidine blue. The ultrathin sections (60 nm thick) were placed in copper grids, selecting the matching area, the corpus callosum below motor cortex, at the fronto-parietal level, and were counterstained with 0.1% lead citrate and 1% uranyl acetate before visualization under electron microscopy (Phillips CM200; Royal Philips Electronics, Amsterdam, The Netherlands). Identical regions were used in both genotypes. Ultrastructurally, the oligodendrocytes were distinguished by morphological criteria, according to their smaller size, greater density of cytoplasm and nucleus (with dense chromatin), absence of intermediate filaments and of glycogen in the cytoplasm, and presence of a large number of microtubules in their processes (Peters et al. 1991; Baumann and Pham-Dinh 2001). As a measure of the myelin integrity, the axonal and fiber diameters were measured and used to calculate the g-ratios (ratio of axonal diameter to fiber diameter, derived from measuring the respective perimeters) (Sherman and Brophy 2005) using ImageJ software (http://imagej.nih.gov/ij/). A minimum of 250 axons per animal was quantified and samples from three animals for each genotype were analyzed. The same sections were used to estimate the proportion of unmyelinated axons with respect to the total, unmyelinated and myelinated axons. The data were analyzed using the t-student test and the Sigma Stat 3.0 and Sigma plot 8.0 software. Values of $p < 0.05$ were considered significant.

## Results

*The lack of $LPA_1$ receptor results in reduced cortical expression of myelin proteins.*

Consistent with previous studies that support a role for *Lpar1* in cortical myelination (Allard et al. 1998; Weiner et al. 1998; Möller et al. 1999; Handford et al. 2001; Cervera et al. 2002), *Lpar1*

was expressed in the cortical adult myelin fibers and oligodendrocytes (see online resource) at its higher level on postnatal day 30 (P30), almost coinciding with the peak of myelination, and declining with age. Both in situ hybridization and immunolabeling were particularly intense in the corpus callosum and at the junction with the cortex in which the immunoreactive fibers and individual oligodendroglial cells were observed (see online resource). Despite this specific pattern of expression, the mice lacking the $LPA_1$ receptor developed structural and apparently functional myelin up to adulthood when the $LPA_1$ immunoreactivity was still intense in the wild-type white matter fibers (not shown). However, as discussed below, a pronounced defective myelination that affected the quantity, quality and organization of the myelinated fibers in the cerebral cortex was observed.

To investigate the effect of the $LPA_1$ deficiency on cortical myelination, we first compared the pattern of myelin proteins in adult (3-month-old) wild-type and null mice. Immunohistochemistry was performed to determine the major protein components in the myelin sheaths, i.e., myelin basic protein (MBP), proteolipid protein (PLP and DM20), and 2', 3'-cyclic nucleotide 3'-phosphodiesterase (CNPase). Because the PLP/DM20 antibody used in this study does not discriminate between the two isoforms, this protein will be referred to by the acronym PLP throughout the remainder of this report. The immunohistochemical qualitative analysis revealed significantly fewer myelinated fibers in mice lacking $LPA_1$ receptor compared with the littermates and age-matched wild-type mice. Myelinated structures such as corpus callosum, fimbria, external capsule and thalamus were immunolabeled extensively and exhibited a similar general pattern in both genotypes, although subtle differences were observed. However, when examined in more detail, a qualitative decrease in the staining of myelin fibers and positive cells was observed in absence of $LPA_1$. This qualitative reduction in stained myelinated fibers was similar for the MBP, CNPase and PLP staining and was more obvious in the cerebral cortex than in the other cerebral

regions (Fig. 1) particularly, in the deep layers in which the fiber density was higher, i.e., the internal granular and infragranular layers (IV-VI), with respect to the upper supragranular layers (I-III), although these layers also exhibited this alteration, as did the striatum, in which affected the overall fiber bundle density and the surrounding small fibers (Fig. 1a-b, e-f, lower and middle panel, respectively). In addition to the appearance of the fibers, the thin-section PLP immunostaining revealed a particular phenotype in the absence of the $LPA_1$ receptor, demonstrating a noticeable accretion of high PLP immunoreactivity in the soma of numerous oligodendrocytes, compared with the wild-type cortex, and was more visible in the spaces devoid of myelin (Fig. 1e, f). The corpus callosum was present and was formed apparently normal in the null mice although it displayed a somewhat disorganized rumpled arrangement of the fibers in $LPA_1$-null mice (Fig. 1e, f, lower panel) compared with the organized rows in wild-type mice. The qualitatively altered pattern of myelination in null animals was corroborated by western blot analysis of the myelin extracts. For this purpose cerebral cortices were dissected and were separated into the cortical superficial region, including layers I-III, and the cortical deep region, containing layers IV-V and where a higher number of myelinated fibers were observed and the major differences were more obvious. Layer VI was excluded to avoid contamination of the sampling with the corpus callosum. Western blot analysis of cortical lysates confirmed the significant reduction in the steady-state levels of cortical myelin proteins in the null mice compared with the age-matched wild-type mice (Fig. 2). GAPDH expression was used to control for the variation in sample loading (Fig. 2a). The expression of the five molecular mass variants (14, 17, 17.2, 18.5, and 21.5 kDa) of the mouse myelin basic protein (MBP), CNPase and PLP (and its splice variant DM20) was decreased significantly ($p < 0.05$) in the majority of the null cortical layers. This reduction was more notable in layers IV-V, in which a reduction of at least 30% to 40% was observed (Fig. 2b, c).

*$LPA_1$-null mice demonstrate MRS evidence of myelination failure.*

Magnetic resonance spectroscopy (MRS) is a non-invasive technique that provides useful information on brain chemistry. MRS offers the opportunity to investigate changes in the metabolite composition of different brains in vivo. The following proton metabolites were investigated in this study: N-acetylaspartate (NAA), found essentially in the neurons, but also in immature oligodendrocytes; phosphocreatine (Cr), considered an index of neuronal density; and choline (Cho), a constituent of membranes and myelin. The Cho/Cr ratio correlates with the cellular density and with choline-containing compounds, which participate in the phospholipid metabolism involved in membrane/myelin synthesis and degradation. An increase in the Cho/Cr ratio is typically associated with increased cell membrane turnover. Usually, the highly organized lipids in myelin are undetectable by MRS. However, in certain states characterized by the breakdown of myelin and other membrane structures, mobile lipids are released and are visible under MRS. Therefore, a higher choline peak suggests active demyelination or evidence of a defect in myelination because of the abundance of choline-containing compounds in the myelin (Bonavita et al. 1999; Khiat et al. 2007).

Based on this observation and our immunochemical results cited previously, MRS was performed on mice of both genotypes at different ages to investigate the in vivo myelin deficiency or malfunction. Figure 3 shows the MR images of the brain from both genotypes representing the voxel locations used for the MRS experiments (Fig. 3a) and the corresponding proton MR spectra (Fig. 3b). The proton spectra exhibited major differences revealing metabolism variations which were a result of the respective genetic backgrounds. Therefore, the MRS data demonstrated a temporal and gradual significant increase in the choline levels (expressed with respect to creatine content) in the brains from $LPA_1$-null mice compared with the wild-type mice (Fig. 3c). The

choline-containing compounds were significantly higher in the null mice from P30 up to P140 compared with the wild-type mice, demonstrating significant differences in all cases ($p < 0.05$) and suggesting myelin alterations as a result of the absence of $LPA_1$ receptor. Whereas the NAA/Cr ratio did not differ significantly among the younger mice, the NAA/Cr ratio increased in the null mice samples, and by P110 and P140 stages, the ratio tended to reach statistical significance ($p < 0.05$) compared with the wild-type mice (Fig. 3c), suggesting that the myelin deficiency was not accompanied by axonal degeneration.

*Absence of $LPA_1$ leads to an increase in unmyelinated axons and myelin g-ratios accompanied by fiber disorganization and altered morphology.*

To investigate further the effects of $LPA_1$ deficiency on cortical myelination at the ultrastructural level, we examined the myelinated axons in equivalent corpus callosum sections from adult mice of both genotypes, selecting the area below motor cortex, at the fronto-parietal level. The corpus callosum was selected because of the higher number and better arrangement of myelinated axons, reducing the occurrence of the other cell types. Ultrastructural analysis of the myelinated axons in matching callosal transverse sections (Fig. 4a, b) demonstrated a significant increase in the percentage of unmyelinated fibers (with respect to the total axon number) in the absence of $LPA_1$ receptor compared with wild-type mice (Fig. 4g) (40.50% ± 2.11% vs. 15.29% ± 1.93%, respectively; $p < 0.01$), and was consistent with the reduction in myelinated fibers observed by immunohistochemistry in other structures of the brain, such as the cerebral cortex, striatum or caudate putamen. In addition, the null mice demonstrated a general disorganized pattern, irregular morphology of fibers and random bundling, which was in contrast with the well-oriented wild-type fibers. This anomalous profile was more obvious in the longitudinal planes (Fig. 4c, d); therefore, whereas the wild-type myelin fibers were oriented in parallel as bundles, the fibers in

the null mice were laid out randomly throughout the corpus callosum, and exhibited different orientations in the same plane (Fig. 4d). In addition, images of aberrant myelin were observed intermittently in the null mutants. Therefore, the periaxonal collar, which normally consists in only one turn of myelin in wild-type, showed fragments of non-compacted myelin in the null mice and was associated with abnormal contours of the myelin bundles (Fig. 4e). Moreover, a number of the null oligodendrocytes contained features resembling the ultrastructural features of apoptosis, showing irregular nuclei and chromatin condensation along the periphery of the nucleus (Fig. 4e, f). Analysis of the g-ratio, i.e. typically the measure of myelin thickness, according to the axon diameter, demonstrated a significant reduction in the degree of myelination in most of the axons in the absence of the $LPA_1$ receptor. Therefore, the g-ratio was significantly higher in the null mice compared with the controls for the axons measuring < 0.5 µm in diameter ($0.80 \pm 0.015$ vs. $0.66 \pm 0.013$, $p < 0.01$), 0.5 µm - 0.7 µm in diameter ($0.84 \pm 0.011$ vs. $0.72 \pm 0.019$, $p < 0.01$) and 0.7 µm - 0.9 µm in diameter ($0.86 \pm 0.013$ vs. $0.76 \pm 0.005$, $p < 0.01$) (Fig. 5h). Similarly, the axonal fibers measuring greater than 9 µm in diameter also exhibited increased g-ratios in the null mice compared with the wild-type mice; however, the increases were not significant. Taken these findings together, we concluded that the myelin integrity, the degree of myelination and the organization of the fibers were affected in the absence of the $LPA_1$ receptor.

*The decrease in the number of differentiating oligodendrocytes in $LPA_1$-null mice is not a result of a reduction in the number of oligodendrocyte progenitors or a developmental anomaly of oligodendroglia*

To determine whether the inadequate myelination of the brain fibers in the cortex was associated with a failure of the oligodendrocyte precursors to differentiate into mature, myelin-producing cells, the numbers of precursors and myelinating cells were estimated using

immunohistochemistry and stereology in the adult and early postnatal mice. Tipically, oligodendrocytes are mostly generated during the first few postnatal weeks in rodents, peaking by postnatal age P7–P14. The oligodendrocytes differentiate from proliferative, migratory oligodendrocyte precursor cells (OPCs) that express a characteristic set of markers of oligodendrocyte lineage, including NG2 proteoglycan, among others, which is rapidly downregulated when the OPCs differentiate into oligodendrocytes (Dimou et al. 2008; Rivers et al. 2008; Kang et al. 2010). Therefore, cortical sections from adult mice of both genotypes were analyzed to calculate the numbers of NG2-expressing glial cells and mature myelinating cells.

We first characterized and identified the mature myelinating oligodendrocytes using immunohistology to detect galactocerebroside (GalC), which is a major component of myelin. GalC immunohistochemistry staining demonstrated a high number of perineuronal oligodendrocytes in both the adult normal and null mice. The number of stained mature oligodendrocytes decreased in the absence of the receptor throughout the entire adult cortex, affecting all layers (Fig. 5a, left panel), as well as in other myelinated areas in which defects in the null mice were evident, such as in the striatum (Fig. 5a, lower left panels). In contrast, immunohistochemical staining for NG2, an earlier marker of the oligodendrocyte lineage, did not reveal significant differences between the genotypes, demonstrating a similar distribution of the OPCs in all the areas analyzed. The density and shape of the OPCs were analyzed throughout the brain, and alterations in the number or shape of the cells were not observed in the absence of $LPA_1$ (Fig. 5a, right panels). To verify these data, the GalC-positive ($Galc^+$) and NG2-positive ($NG2^+$) cells in the primary and secondary motor cortex were counted through the rostral-caudal extension (Fig. 5b, c). The numerical density of the cells (*N*v) in the motor cortex was determined in the adult brains for both genotypes using the optical dissector method (West 1993). The analysis demonstrated that the number of $GalC^+$ mature myelinating cells was decreased significantly in

the absence of the $LPA_1$ receptor (wild-type *N*v = 491,825.4 ± 52,300.1; null *N*v = 333,571.2 ± 54,406.3; *N*v, cells/$mm^3$; $p < 0.05$) (Fig. 5b) whereas the density of the $NG2^+$ OPCs did not differ between both genotypes (wild-type *N*v = 51,197.7 ± 2,658.6; null *N*v = 52,305.2 ± 1,617.0; *N*v, cells/$mm^3$; $p < 0.05$) (Fig. 5c) suggesting that there was no deficit in the number of OPCs available to develop into mature myelinating cells.

These alterations were investigated in the adult mice; however the myelination process begins at birth and develops during the first month of life. A possible explanation for many of these $LPA_1$-dependent defects is that they are a consequence of anomalous oligodendroglial development. Therefore, to discriminate their origin as well as the role of LPA in myelination, the same experiments were performed in mice at two different younger stages, focusing on the alterations in the motor cortex where the reduction in myelinated fibers and oligodendrocytes was more evident in the adult mice. The first age chosen, postnatal day 10 (P10), was directly before the peak in the expression of $LPA_1$ (P18), which coincides with the period when myelinization is most active (Weiner et al. 1998). The other stage investigated was when the myelination processes had just ended, P30 (Nakahara et al. 2001).

By P30, the differences in the myelination pattern between the genotypes, normal and null, were quite similar to those reported throughout adult brain. Unlike the wild-type cortex (Fig. 6a), the cerebral cortices from the null mice exhibited reduced densities of the MBP-positive ($MBP^+$) fibers and the accumulation of PLP-positive ($PLP^+$) intense immunoreactivity in many oligodendrocyte soma (Fig. 6b). The perinuclear accretion of PLP-positive material was also evident in other areas of the brain in the null mice, such as the striatum (Fig. 6b), whereas in the wild-type brain, the moderate staining of the $PLP^+$ material appeared equally in the oligodendroglial processes and soma (Fig. 6a). In contrast, before the onset of myelination (P10), no significant differences were detected between the null and wild-type mice (Fig. 7a). The

distribution and intensity of the nascent $MBP^+$ myelin fibers (Fig. 7a, b, left panels) were similar in both genotypes, occupying the lower half of the cortical wall and suggesting the absence of myelination defects in the mice lacking the $LPA_1$ receptor. Likewise, the detection of PLP expression, which occurred shortly after the expression of MBP (Monge et al. 1986), demonstrated similar densities of $PLP^+$ cells in both genotypes; importantly, this protein still remained in the soma, according to this early stage (Fig. 7a, b, right panels). The analysis of the $NG2^+$ OPCs and $GalC^+$ myelinating cells in the P10 motor cortex by immunohistochemistry (Fig. 7c, d) and stereology (Fig. 7e, f) confirmed the absence of $LPA_1$-dependent developmental defects, showing similar myelinating cell densities (wild-type *N*v = 510,552.4 ± 15,915.3; null *N*v = 528,778.9 ± 12,641.5; *N*v, cells/$mm^3$; $p < 0.05$) (Fig. 7e) and oligodendrocyte precursors (wild-type *N*v = 100,501.6 ± 7,213.4; null *N*v = 108,822.3 ± 11,460.5; *N*v, cells/$mm^3$; $p < 0.05$) (Fig. 7f) in both genotypes. Therefore, we concluded that the deficits in the mature myelinating oligodendrocytes from the ma$LPA_1$-null mice did not appear associated with development and coincided with the normal time for the onset of major myelination and the highest expression of the $LPA_1$ receptor.

*The lack of $LPA_1$ receptor generates anomalous trafficking of proteolipid protein and induces apoptosis in the oligodendrocyte*

Oligodendrocytes synthesize and transport large amounts of myelin membrane by means of an intricate cell polarity, establishing discrete membrane trafficking pathways that allow the directed transport of myelin components to the axon. To construct myelin sheaths, oligodendrocytes guide myelin proteins in different ways. Therefore, whereas MBP is synthesized on free polyribosomes located at the sites of myelin sheath assembly, PLP molecules are synthesized and processed in the rough endoplasmic reticulum (RER)/Golgi apparatus complex located in the perinuclear

cytoplasm (Colman et al. 1982; Trapp et al. 1987). Whereas MBP is essential for myelination, PLP appears dispensable because in the absence of PLP, oligodendrocytes still myelinate. Nevertheless, previous studies have demonstrated that PLP is critical for stabilizing and assembling the myelin membrane structure upon compaction (Klugmann et al. 1997).

In this study, PLP was affected in the absence of the $LPA_1$ receptor, suggesting subcellular deficits that could affect the overall process of myelination. Therefore, although most of the cortical oligodendrocytes from the adult wild-type animals exhibited moderate immunostaining for PLP, which was uniformly distributed, and labeled equally the soma and cell processes (Fig. 1e, 7a), myelinating cells from the adult null mice demonstrated a more restricted distribution of the $PLP^+$ label, which localized preferentially around the soma (Fig. 1f, 7b). As demonstrated previously, these differences in PLP immunoreactivity were associated with the genotype and appeared during adulthood, just after the highest expression level for $LPA_1$. This PLP distribution in the $LPA_1$-null oligodendrocytes indicated that the PLP molecules were retained largely in the oligodendrocyte soma; therefore, we quantified the $PLP^+$ cells and characterized the PLP subcellular distribution to better understand its relevance in the observed myelin defects.

According to the distribution of immunoreactivity, the oligodendrocytes from both genotypes were classified as follows: oligodendrocytes expressing the properties of normal oligodendrocytes ('normal'), demonstrating moderate PLP immunoreactivity that was equally distributed in the soma and cell processes (more frequent in the wild-type mice); and oligodendrocytes exhibiting the accumulation of intense PLP immunoreactivity in the perinuclear soma ('intense') that were observed predominantly in the null mice or in the early normal oligodendrocyte development, before myelination. Similar to the previous stereological analyses, the number of $PLP^+$ cells in the motor cortex was counted through the rostral-caudal extension to determine the numerical density ($N_v$). The analysis confirmed a significant reduction (almost 30%) in the total $PLP^+$ cells in the

$LPA_1$-null cortex (wild-type *N*v = 313,057.7± 21,778.4; null *N*v = 222,568.3 ± 21,637.1; *N*v, cels/$mm^3$; $p < 0.05$) (Fig. 8a), which was consistent with the previous data for the adult $GalC^+$ cells. In addition, the $PLP^+$ 'intense' cells were notably numerous in the absence of the $LPA_1$ receptor, compared with the normal mice (wild-type *N*v = 49,941.3± 7,809.5; null *N*v = 66,058.1 ± 2,590.2; *N*v, cels/$mm^3$; $p < 0.05$) (Fig. 8a).

PLP, unlike MBP or CNPase, is synthesized in the RER, is subsequently transported via vesicles through the Golgi apparatus (GA), and is sorted to the plasma membrane, where the translated protein is inserted into myelin rafts (Colman et al. 1982; Trapp et al. 1987). Based on the cell count data and the suggested LPA-mediated effect on the oligodendrocyte cytoskeletal rearrangements involved in the membrane sheath formation (Nogaroli et al. 2009), a reasonable hypothesis is that $LPA_1$ signaling plays a significant role in PLP transport; therefore, we investigated the stage along the pathway in which PLP was retained in the null oligodendrocytes. Double-immunofluorescence staining was performed to investigate PLP protein localization relative to the following markers in each cell compartment: i) protein disulfide isomerase (PDI), an abundant endoplasmic reticulum chaperone protein that catalyzes disulfide-bond breakage and formation and is normally used as an RER marker (Wang et al. 1998); ii) Golgi phosphoprotein (Golph4), a transmembrane protein localized to the cis-Golgi cisternae and a marker of early Golgi vesicle trafficking (Linstedt et al. 1997); and iii) Lamp1, a type-I transmembrane glycoprotein that is localized primarily in lysosomes and late endosomes (Rohrer et al. 1996), based on the observation that newly synthesized molecules are typically transported from the trans-Golgi network directly to the endosomes and, subsequently, to the lysosomes.

Compared to the controls, the merged staining from the cortical oligodendrocytes lacking $LPA_1$ demonstrated PLP retention within the RER (Fig. 8b, top row) and in the cis-Golgi, although not completely (Fig. 8b, middle row). Therefore, whereas PDI and PLP were colocalized mostly in the

null cells (Fig. 8b, top row), suggesting that part of the PLP protein was trapped within the RER, in the normal mice, the PLP was barely present in this organelle after synthesis (Fig. 8b, top row). Likewise, whereas Golph4 and PLP were not colocalized in the wild-type oligodendroglial cells, a considerable amount of PLP immunoreactivity were found in the Golgi cisternae in the null oligodendrocytes, although the colocalization was not absolute in all cells (Fig. 8b, middle row), suggesting that PLP remained in the Golgi-network temporarily and was recycled continuously. Finally, the colocalization pattern of Lamp1 and PLP exhibited a similar distribution pattern, demonstrating that in contrast to the wild-type cells, PLP and Lamp1 were colocalized in the majority of the $LPA_1$-null oligodendrocytes (Fig. 8b, bottom row). Lysosomes are known to link protein biosynthetic and degradation pathways, and are involved in secretion, membranes turnover, and endocytosis. Lysosomes also play multifunctional roles in sorting, processing and degradation. Therefore, it is difficult to discern whether the localization of PLP in lysosomal vesicles was because of normal transport towards the membrane or as part of degradation pathways induced by protein accumulation.

Based on the data, our logical conclusion was that the increase in the PLP protein in the membrane system of the oligodendrocyte induced deleterious effects in the cells. Because previous studies have reported that disrupted PLP trafficking and the accumulation of a number of myelin proteins trigger endoplasmic reticulum stress-induced apoptosis in oligodendrocytes (Gow et al. 1998; Lin and Popko 2009), we investigated whether these defects in the ma$LPA_1$-null mice were responsible for the increased apoptosis. To address this question, the apoptosis was measured in the motor cortical area in both genotypes. TUNEL staining demonstrated a consistent increase in the number of apoptotic nuclei in the mice lacking the $LPA_1$ receptor, compared with the wild-type mice (Fig. 9a). The number of stained nuclei demonstrated significant differences between genotypes; an increase in apoptosis of approximately 28% was observed in the null mice (wild-

type *N*v = 39,403.1 ± 354.1; null *N*v = 50,385.2 ± 2,213.5; *N*v, cels/mm$^3$; $p < 0.05$) (Fig. 9c). Given the difficulty associated with the immunohistological classification of the apoptotic cells, mainly because of significant cell degradation and the loss of protein expression (Sohn et al. 2012), we analyzed the percentage of apoptotic nuclei in the corpus callosum, an area in which the oligodendroglial population predominates. The data confirmed the increased presence of apoptotic nuclei in the callosal sections from the $LPA_1$-null mice (Fig. 9b) and a significant increase in the fraction of apoptotic cells, estimated as the TUNEL-positive signal relative to the counterstained nuclei within each tissue section (wild-type, 1.9 ± 0.3; null, 3.9 ± 0.8; $p < 0.05$) (Fig. 9d). Therefore, these findings suggested that the myelin and PLP trafficking defects caused by the absence of the $LPA_1$ receptor in the oligodendrocyte eventually lead to cell death and demonstrated the relevance of this receptor in myelination in the cerebral cortex.

**Discussion**

As reported previously, $LPA_1$ expression is correlated largely with the expression of myelin proteins, suggesting that the protein plays an important role in myelination (Allard et al. 1998; Weiner et al. 1998; Möller et al. 1999; Handford et al. 2001; Cervera et al. 2002), which is supported by pharmacological evidence (Möller et al. 1999; Stankoff et al. 2002; Dawson et al. 2003; Matsushita et al. 2005; Nogaroli et al. 2009). However, with the exception of studies (Contos et al. 2000) demonstrating a minor increase in apoptosis in Schwann cells from $LPA_1$-null mice, there are limited data and no in vivo evidence to support a role for $LPA_1$ in this function. This study is the first to demonstrated an in vivo requirement and functional contribution for the $LPA_1$ receptor in cortical oligodendrocyte maturation and myelination via the analysis of the

*Málaga* variant maLPA$_1$-null mice. The mice generated normal numbers of oligodendrocytes, which initiated normal myelination (Fig. 7). However, as the cells reached later stages of myelination, they failed to regulate the myelin proteins (Figs. 1 and 2) and showed ultrastructural anomalies (Fig. 4), demonstrating that the deficits were restricted to maturing myelinating oligodendrocytes and that LPA$_1$-signaling was a late-stage regulator of myelination.

A number of our findings were based on non-invasive approaches, i.e. the MRS provided a reliable in vivo functional scenario to test for the absence of the receptor. The MRS demonstrated significant alterations in the metabolite levels in the null mice. The ratio of choline to creatine (Cho/Cr) is particularly relevant to the study of the white matter state. Increases in Cho/Cr are considered an indication of increased cell membrane turnover, axonal degeneration and active demyelination, and have been reported in many pathological degenerative conditions, such as in active multiple sclerosis plaques (Miller et al. 1991; Simone et al. 1996). The absence of the LPA$_1$ receptor resulted in increased Cho/Cr ratios, which is consistent with the presence of myelin alterations and oligodendroglial death. However the augmentation of the choline levels was accompanied by a significant increase in NAA at the later stages, suggesting the absence of active degenerative episodes. Elevations in the Cho/Cr ratio have also been reported in non-degenerative conditions, as indications of hypomyelination (Filippi et al. 2002). Furthermore, shiverer mice, do not exhibit axonal degeneration although they are severely dysmyelinated (Griffiths et al. 1998). Additionally, the NAA increase argues against the possibility that the myelin defects in certain cortical layers could also partially reflect the reduction in cortical neurons in the deepest layers reported in the null mice (Estivill-Torrús et al. 2008). In this sense, 200 kD neurofilament immunostaining to detect all axons in the tissue (both phosphorylated and non-phosphorylated epitopes of neurofilament proteins, which are thought to be necessary for the maintenance of neurons with myelinated processes) did not demonstrate substantial differences between the two

genotypes at the cortical level (see online resource), which supports the absence of axonal degeneration/decrease influencing the observed change in the steady-state levels of the myelin proteins. Raised NAA levels have also been detected in the brain under certain conditions in diseases not associated with neuronal proliferation, such as Canavan disease, Pelizaeus-Merzbacher disease, familial bipolar I disorder and sickle cell disease, suggesting other than neuronal contribution for the NAA increase (Steen and Ogg 2005). Nevertheless, excluding pathological circumstances, we can cautiously interpret the NAA increase as a result of the reported oligodendroglial abnormalities (Urenjak et al. 1992), especially considering that NAA is hydrolyzed by amidohydrolase II, which is present in oligodendrocytes, and that the majority of these hydrolysis-derived compounds appear to be taken up and metabolized by oligodendrocytes or astrocytes (Warringa et al. 1987; Baslow et al. 2003). Additionally, because NAA provides acetyl groups for lipid synthesis during myelination and demyelination is attributed to a deficiency in the enzyme N-acetylaspartoacylase, some authors have suggested a relationship between altered myelination and an increase in NAA (Bhakoo and Pearce 2000).

The absence of PLP causes abnormal myelin compaction (Klugmann et al. 1997; Rosenbluth et al. 2006). Accordingly, the $LPA_1$-null mice exhibited alterations in the compaction and composition of the lamellae, which demonstrated a reduction in the steady-state levels of the three primary myelin proteins MBP, PLP and CNPase in the cortex. These data are consistent with the suggested role for $LPA_1$ in influencing the expression or translation of PLP during oligodendrocyte differentiation (Weiner et al. 1998) and the induction of membranous processes involving MBP (Nogaroli et al. 2009). Indeed, the expression of not only PLP and MBP but also O4, CNPase and GalC has been associated with $LPA_1$ activation (Matsushita et al. 2005). Nevertheless, based on the $LPA_1$-dependent defects in PLP/DM20 trafficking and the western blot data and because PLP interacts with MBP (Fannon and Moscarello 1990) and has been suggested to facilitate the

transport of other cargo proteins into the myelin (Werner et al. 2007), we cannot rule out the possibility that PLP indirectly affects the other myelin components. Moreover, the suggested role for $LPA_1$ in regulating PLP/DM20 and myelination is even more significant considering myelin genes are influenced by the state of myelination and gene-dosage and that the increase in the levels of PLP/DM20 caused the retention of the protein in the oligodendrocyte soma and the reduction of other myelin proteins, particularly MBP (Karim et al. 2007). The retention of the PLP/DM20 protein in the endoplasmic reticulum in the ma$LPA_1$-null mice and the subsequent defective myelination and oligodendrocyte death are, in a number of ways, consistent with similar features reported in *Plp1* mouse mutants (Griffiths et al. 1998; McLaughlin et al. 2006a,b; Southwood and Gow 2001; Southwood et al. 2002). Therefore, it is important to elucidate the molecular influence of $LPA_1$ on PLP/DM20, and to emphasize the clinical relevance of these processes in the pathogenesis of myelin disorders, including Charcot-Marie-Tooth disease, Pelizaeus-Merzbacher disease, vanishing white matter disease, and multiple sclerosis (Lin and Popko 2009). Alternatively, we cannot exclude that the $LPA_1$-dependent defects in oligodendrocyte maturation and other factors influence intracellular PLP transport, e.g., axonal plasticity, which induces changes in myelin composition (Drøjdahl et al. 2010). In either case, given the role myelinating glial cells play in supporting axonal integrity (Edgard et al. 2009; Edgard and Nave, 2009; Nave 2010), an ultimately attractive scenario would be one in which LPA modulates both plasticity (reviewed in Noguchi et al. 2009; Choi et al. 2010; Choi and Chun 2013) and myelination in a bidirectional manner through $LPA_1$.

Considering the important contribution of cortical myelin deficiency in many neurological diseases, the relevance of callosal abnormalities implies behavioral consequences. The corpus callosum is a large fiber network connecting the cerebral hemispheres and is characterized by fiber density and myelination levels that reflect the functional specialization. Because structural

alterations in the corpus callosum involve axonal connections between the association cortices, the consequences are variable neural and behavioral effects, depending on the situation (van der Knaap and van der Ham 2011). Consequently, not only cortico-cortical disconnection disruptions affecting sensorimotor coordination but also abnormalities affecting fiber, myelin, and/or cellular integrities have been associated with schizophrenia (Keshavan et al. 2002; Tkachev et al. 2003; Whitford et al. 2010), stress disorders (Villareal et al. 2004; Miyata et al. 2011), and cocaine consumption (Ma et al. 2009; Narayana et al. 2009), contributing to the development of the pathological condition to a greater or lesser degree. Interestingly, in this sense, maLPA$_1$-null mice have been shown to i) develop deficits in motor impairments, which affects neuromuscular strength and the analgesic response (Santín et al. 2009); ii) share anatomical, neurochemical and behavioral abnormalities resembling those found in schizophrenia (Roberts et al. 2005; Estivill-Torrús et al. 2013); iii) acquire increased vulnerability to chronic stress-neural effects (Castilla-Ortega et al. 2011); and iv) exhibit altered conditioned responses to cocaine (Blanco et al. 2012), suggesting the contribution of the defects described in this study to the development of these phenotypes.

Regardless of the specific LPA$_1$-dependent oligodendroglial deficiencies, myelination is a well orchestrated multicellular process involving glial-neuronal interactions and intrinsic and extrinsic signaling mechanisms (Emery et al. 2010). The LPA receptors are expressed in the majority of brain neural cell types (reviewed in Choi et al. 2010; Choi and Chun 2013). Although LPA$_1$ is expressed predominantly in oligodendrocytes in the adult brain, underscoring its role in myelination, we cannot exclude the indirect participation of other CNS LPA$_1$-expressing cell types, such as astrocytes, which induce LPA-dependent indirect effects on neuronal differentiation (Spohr et al. 2008, 2011) and have important roles in efficient myelination and oligodendrocyte differentiation (Ishibashi et al. 2006; Sorensen et al. 2008; Watkins et al. 2008; Moore et al. 2011).

Similarly, many other signaling factors influencing the overall process may be important. Recently, a significant role for the signaling molecules extracellular signal-regulated protein kinases 1 and 2 (ERK1/ERK2), mediators of mitogen-activated protein kinases (MAPKs), has been demonstrated for the control of CNS myelin thickness (Ishii et al. 2012). Interestingly, LPA modulates ERK1/2 activation in oligodendrocytes (Stankoff et al. 2002; Yu et al. 2004), suggesting that further studies will be necessary to establish the complete $LPA_1$-effectors route in the oligodendrocyte scenario. Nevertheless, although the precise signaling cascades through which LPA elicits its functions in this context will require further investigation, our results are the first to provide insights into the in vivo mechanism of the $LPA_1$ receptor in oligodendrocytes and in myelination, suggesting that strategies to regulate $LPA_1$ expression might represent a reliable and promising therapeutic strategy to promote endogenous remyelination. In this sense, remarkably, the proteomic analysis of cerebrospinal fluid samples from multiple sclerosis patients has demonstrated the upregulation of autotaxin, the enzyme responsible for LPA synthesis (Hammack et al. 2004). In conclusion, the absence of the $LPA_1$ receptor in a viable mouse model resulted in alterations in the myelination process in young mice, affecting myelin component trafficking and the myelin structure of cortical efferent axons as well as oligodendrocyte survival. These findings will help elucidate the alterations to myelin and the contribution of LPA signaling to the myelination process under normal and pathological conditions.

**Funding:** This work was supported by the Carlos III Health Institute, State Department of Research, Development and Innovation, Spanish Ministry of Economy and Competitiveness (grant numbers PI10/02514 -co-funded by European Research Development Fund-, to G.E-T.; SAF2011 to IV-N); Andalusian Regional Ministries of Health (Nicolás Monardes Programme, and grants PI0187/2008, PI0232/2007 to G.E-T.) and of Economy, Innovation, Science and

Employment (CTS643 and CTS433 research group grants to G.E-T. and F.R-DF., respectively); Ramon Areces Foundation (Ramon Areces Fellowship to B.G-D.); and the National Institutes of Health (USA) (grant numbers MH051699 and MH01723 to J.C.).

**Notes:** We gratefully acknowledge IBIMA joint services, common support structures for research (ECAI) of General Services, Microscopy and Animal Experimentation, for management, immunohistology and maintenance of mice, respectively, as well as technical assistance. Likewise we are obliged to central microscopy facilities at Universidad de Málaga for confocal and electron microscopy. The authors declare that they have no conflict of interest.

## References

Allard J, Barron S, Diaz J, Lubetzki C, Zalc B, Schwartz JC, Sokoloff P (1998) A rat G protein-coupled receptor selectively expressed in myelin-forming cells. Eur J Neurosci 10:1045-1053

Anliker B, Chun J (2004) Lysophospholipid G protein-coupled receptors. J Biol Chem 279:20555-20558

Anliker B, Choi JW, Lin ME, Gardell SE, Rivera RR, Kennedy G, Chun J (2013) Lysophosphatidic acid (LPA) and its receptor, LPA1, influence embryonic schwann cell migration, myelination, and cell-to-axon segregation. Glia 61: 2009-2022

Baslow MH (2003) N-Acetylaspartate in the Vertebrate Brain: Metabolism and Function. Neurochem Res 28:941-953

Baumann N, Pham-Dinh D (2001) Biology of oligodendrocyte and Myelin in the Mammalian Central Nervous System. Physiol Rev 81: 871-927

Bhakoo KK, Pearce D (2000) In vitro expression of N-acetyl aspartate by oligodendrocytes: implications for proton magnetic resonance spectroscopy signal in vivo. J Neurochem 7:254-262

Birgbauer E, Chun J (2006) New developments in the biological functions of lysophospholipids. Cell Mol Life Sci 63:2695-2701

Blanco E, Bilbao A, Luque MJ, Palomino A, Bermudez-Silva FJ, Suarez J, Santin L, Gutierrez A, Campos-Sandoval JA, Marquez J, Estivill-Torrus G, Rodriguez De Fonseca F (2012) Lack of cocaine-induced conditioned locomotion is associated with altered expression of hippocampal glutamate receptors in mice lacking lpa1 receptor. Psychopharmacol 220:27-42

Bonavita S, Di Salle F, Tedeschi G (1999) Proton MRS in neurological disorders. Eur J Radiol 30:125-131

Brinkmann V, Lynch KR (2002) FTY720: Targeting G-protein-coupled receptors for sphingosine 1-phosphate in transplantation and autoimmunity. Curr Opin Immunol 14:569-575

Castilla-Ortega E, Sánchez-López J, Hoyo-Becerra C, Matas Rico E, Zambrana-Infantes E, Chun J, Rodríguez de Fonseca F, Pedraza C, Estivill-Torrús G, Santín LJ (2010) Activity, anxiety and spatial memory impairments are dissociated in mice lacking the LPA1 receptor. Neurobiol Learn Mem 94:73-82

Castilla-Ortega E, Hoyo-Becerra C, Pedraza C, Chun J, Rodríguez de Fonseca F, Estivill-Torrús G, Santín LJ (2011) Aggravation of the Pathological Consequences of Chronic Stress on Hippocampal Neurogenesis and Spatial Memory in Mice Lacking the LPA1 Receptor. PLoS One 6 (9):e25522

Castilla-Ortega E, Pedraza C, Chun J, Rodríguez de Fonseca F, Estivill-Torrús G, Santin LJ (2012) Hippocampal c-Fos activation in normal and LPA1-null mice after two object recognition tasks with different memory demands. Behav Brain Res 232:400-405

Cervera P, Tirard M, Barron S, Allard J, Trottier S, Lacombe J, Daumas-Duport C, Sokoloff P (2002) Immunohistological localization of the myelinating cell-specific receptor LP(A1). Glia 38:126-136

Choi JW, Herr DR, Noguchi K, Yung YC, Lee CW, Mutoh T, Lin ME, Teo ST, Park KE, Mosley AN, Chun J (2010) LPA receptors: subtypes and biological actions. Annu Rev Pharmacol Toxicol 50:157-186

Choi JW, Chun J (2013) Lysophospholipids and their receptors in the central nervous system. Biochim Biophys Acta 1831:20-32

Chun J (2005) Lysophospholipids in the nervous system. Prostaglandins Other Lipid Mediat 77:46-51.

Chun J, Rosen H (2006) Lysophospholipid receptors as potential drug targets in tissue transplantation and autoimmune diseases. Curr Pharm Des. 12:161-171

Colman DR, Kreibich G, Frey AB, Sabatini D D. 1982. Synthesis and incorporation of myelin polypeptides into CNS myelin. J Cell Biol 95:598-608

Contos JJ, Chun J (1998) Complete cDNA sequence, genomic structure, and chromosomal localization of the LPA receptor gene, lpA1/vzg-1/Gpcr26. Genomics 51:364-378

Contos JJ, Fukushima N, Weiner JA, Kaushal D, Chun J (2000) Requirement for the lpA1 lysophosphatidic acid receptor gene in normal suckling behavior. Proc Natl Acad Sci USA 97:13384-13389

Dawson J, Hotchin N, Lax S, Rumsby M (2003) Lysophosphatidic acid induces process retraction in CG-4 line oligodendrocytes and oligodendrocyte precursor cells but not in differentiated oligodendrocytes. J Neurochem 87:947-957

Dennis D, White MA, Forrest AD, Yuelling LM, Nogaroli L, Afshari FS, Fox MA, Fuss B (2008) Phosphodiesterase- I/Autotaxin's MORFO domain regulates oligodendroglial process network formation and focal adhesion organization. Mol Cell Neurosci 37:412-424

Dimou L, Simon C, Kirchhoff F, Takebayashi H, Götz M (2008) Progeny of Olig2-expressing progenitors in the gray and white matter of the adult mouse cerebral cortex. J Neurosci 28:10434-10442

Drøjdahl N, Nielsen HH, Gardi JE, Wree A, Peterson AC, Nyengaard JR, Eyer J, Finsen B (2010) Axonal plasticity elicits long-term changes in oligodendroglia and myelinated fibers. Glia 58:29-42

Edgar JM, McLaughlin M, Werner HB, McCulloch MC, Barrie JA, Brown A, Faichney AB, Snaidero N, Nave KA, Griffiths IR (2009) Early ultrastructural defects of axons and axon-glia junctions in mice lacking expression of Cnp1. Glia 16:1815-1824

Edgar JM, Nave KA (2009) The role of CNS glia in preserving axon function. Curr Opin Neurobiol 19:498-504

Emery B (2010) Regulation of oligodendrocyte differentiation and myelination. Science 330:779-782

Estivill-Torrús G, Llebrez-Zayas P, Matas-Rico E, Santín L, Pedraza C, De Diego I, Del Arco I, Fernández-Llebrez P, Chun J, Rodríguez de Fonseca F (2008) Absence of LPA1 signaling results in defective cortical development. Cereb Cortex 18:938-950

Estivill-Torrús G, Santín LJ, Pedraza C, Castilla-Ortega E, Rodriguez de Fonseca F (2013) Role of Lysophosphatidic Acid (LPA) in Behavioral Processes: Implications for Psychiatric Disorders. In: Chun J (ed) Lysophospholipid Receptors: Signaling and Biochemistry. John Wiley & Sons Inc, New Jersey, pp 451-474

Fannon AM, Moscarello MA (1990) Myelin basic protein is affected by reduced synthesis of myelin proteolipid protein in the jimpy mouse. Biochem J 268:105-110

Filippi CG, Uluğ AM, Deck MD, Zimmerman RD, Heier LA (2002) Developmental delay in children: assessment with proton MR spectroscopy. Am J Neuroradiol 23:882-888

Fox MA, Colello RJ, Macklin WB, Fuss B (2003) Phosphodiesterase-Ialpha/autotaxin: a counteradhesive protein expressed by oligodendrocytes during onset of myelination. Mol Cell Neurosci 23:507-519

García-Fernández M, Castilla-Ortega E, Pedraza C, Blanco E, Hurtado-Guerrero I, Barbancho MA, Chun J, Rodríguez-de-Fonseca F, Estivill-Torrús G, Santín Núñez LJ (2012) Chronic immobilization in the malpar1 knockout mice increases oxidative stress in the hippocampus. Int J Neurosci 122:583-589

Gow A, Southwood CM, Lazzarini RA (1998) Disrupted proteolipid protein trafficking results in oligodendrocyte apoptosis in an animal model of Pelizaeus-Merzbacher disease. J Cell Biol 140:925-934

Griffiths I, Klugmann M, Anderson T, Yool D, Thomson C, Schwab MH, Schneider A, Zimmermann F, McCulloch M, Nadon N, Nave KA (1998) Axonal swellings and degeneration in mice lacking the major proteolipid of myelin. Science 280:1610-1613

Gundersen HJ, Bagger P, Bendtsen TF, Evans SM, Korbo L, Marcussen N, Moller A, Nielsen K, Nyengaard JR, Pakkenberg B, Sorensen FB, Vesterby A, West MJ (1988). The new stereological tools: dissector, fractionator, nucleator and point sampled intercepts and their use in pathological research and diagnosis. Acta Pathol Microbiol Immunol Scand 96: 857-881

Hammack BN, Fung KY, Hunsucker SW, Duncan MW, Burgoon MP, Owens GP, Gilden DH (2004) Proteomic analysis of multiple sclerosis cerebrospinal fluid. Mult Scler 10:245-260

Handford EJ, Smith D, Hewson l, McAllister G, Beer MS (2001) Edg2 receptor distribution in adult rat brain. Neuroreport 12:757-760

Ishii A, Fyffe-Maricich SL, Furusho M, Miller RH, Bansal R (2012) ERK1/ERK2 MAPK signaling is required to increase myelin thickness independent of oligodendrocyte differentiation and initiation of myelination. J Neurosci 32:8855-8864

Ishibashi T, Dakin KA, Stevens B, Lee PR, Kozlov SV, Stewart CL, Fields RD (2006) Astrocytes promote myelination in response to electrical impulses. Neuron 49:823-832

Karim SA, Barrie JA, McCulloch MC, Montague P, Edgar JM, Kirkham D, Anderson TJ, Nave KA, Griffiths IR, McLaughlin M (2007) PLP overexpression perturbs myelin protein composition and myelination in a mouse model of Pelizaeus-Merzbacher disease. Glia 55:341-351

Keshavan MS, Diwadkar VA, Harenski K, Rosenberg DR, Sweeney JA, Pettegrew JW (2002) Abnormalities of the corpus callosum in first episode, treatment naive schizophrenia. J Neurol Neurosurg Psychiatry 72:757-760

Khiat A, Lesage J, Boulanger Y (2007) Quantitative MRS study of Baló's concentric sclerosis lesions. Magn Reson Imaging 25:1112-1115

Klugmann M, Schwab MH, Pühlhofer A, Schneider A, Zimmermann F, Griffiths IR, Nave KA (1997) Assembly of CNS myelin in the absence of proteolipid protein. Neuron 18:59-70

Lin ME, Herr DR, Chun J (2010) Lysophosphatidic acid (LPA) receptors: signaling properties and disease relevance. Prostaglandins Other Lipid Mediat 91:130-138

Lin W, Popko B (2009) Endoplasmic reticulum stress in disorders of myelinating cells. Nat Neurosci 212:379-385

Linstedt AD, Mehta A, Suhan J, Reggio H, Hauri HP (1997) Sequence and overexpression of GPP130/GIMPc: evidence for saturable pH-sensitive targeting of a type II early Golgi membrane protein. Mol Biol Cell 8:1073-1087

Ma L, Hasan KM, Steinberg JL, Narayana PA, Lane SD, Zuniga EA, Kramer LA, Moeller FG (2009) Diffusion tensor imaging in cocaine dependence: regional effects of cocaine on corpus callosum and effect of cocaine administration route. Drug Alcohol Depend 104:262-267

Matas-Rico E, García-Díaz B, Llebrez-Zayas P, López-Barroso D, Santín L, Pedraza C, Fernández-Llebrez P, Téllez T, Redondo M, Chun J, Rodríguez de Fonseca F, Estivill-Torrús G (2008) Deletion of lysophosphatidic acid receptor LPA1 reduces neurogenesis in the mouse dentate gyrus. Mol Cell Neurosci 39:342–355

Matsushita T, Amagai Y, Soga T, Terai K, Obinata M, Hashimoto S (2005) A novel oligodendrocyte cell line OLP6 shows the successive stages of oligodendrocyte development: late progenitor, immature and mature stages. Neuroscience 136:115-121

McLean IW, Nakane PK (1974) Periodate-lysine-paraformaldehyde fixative. A new fixative for immunoelectronmicroscopy. Histochem Cytochem 22:1077

McLaughlin M, Barrie JA, Karim SA, Montague P, Edgar JM, Kirkham D, Thomson CE, Griffiths IR (2006a) Processing of PLP in a model of Pelizaeus-Merzbacher disease/SPG2 due to the rumpshaker mutation. Glia 53:715-722

McLaughlin M, Karim SA, Montague P, Barrie JA, Kirkham D, Griffiths IR, Edgar JM (2006b) Genetic background influences UPR but not PLP processing in the rumpshaker model of PMD/SPG2. Neurochem Res 32:167-176

Miller DH, Austin SJ, Connelly A, Youl BD, Gadian DG, McDonald WI (1991) Proton magnetic resonance spectroscopy of an acute and chronic lesion in multiple sclerosis. Lancet 337:58-59

Miyata S, Koyama Y, Takemoto K, Yoshikawa K, Ishikawa T, Taniguchi M, Inoue K, Aoki M, Hori O, Katayama T, Tohyama M (2011) Plasma corticosterone activates SGK1 and induces morphological changes in oligodendrocytes in corpus callosum. PLoS One 6:e19859

Möller T, Musante DB, Ransom BR (1999) Lysophosphatidic acid-induced calcium signals in cultured rat oligodendrocytes. Neuroreport 10:2929-2932

Monge M, Kadiiski D, Jacque CM, Zalc B (1986) Oligodendroglial expression and deposition of four major myelin constituents in the myelin sheath during development. An in vivo study. Dev Neurosci 8:222-235

Moolenar WH, van Meeteren LA, Giepmans BNG (2004) The ins and outs of lysophosphatidic acid signaling. BioEssays 26:870-881

Moore CS, Milner R, Nishiyama A, Frausto RF, Serwanski DR, Pagarigan RR, Whitton JL, Miller RH, Crocker SJ (2011) Astrocytic tissue inhibitor of metalloproteinase-1 (TIMP-1) promotes oligodendrocyte differentiation and enhances CNS myelination. J Neurosci 31:6247-6254

Nakahara J, Tan-Takeuchi K, Seiwa C, Yagi T, Aiso S, Kawamura K, Asou H (2001) Myelin basic protein is necessary for the regulation of myelin-associated glycoprotein expression in mouse oligodendroglia. Neurosci Lett 298:163-166

Narayana PA, Ahobila-Vajjula P, Ramu J, Herrera J, Steinberg JL, Moeller FG (2009) Diffusion tensor imaging of cocaine-treated rodents. Psychiatry Res 171:242-251

Nave KA (2010) Myelination and support of axonal integrity by glia. Nature 468: 244-252

Nogaroli L, Yuelling LM, Dennis J, Gorse K, Payne SG, Fuss B. (2009) Lysophosphatidic acid can support the formation of membranous structures and an increase in MBP mRNA levels in differentiating oligodendrocytes. Neurochem Res 34:182-193

Noguchi K, Herr D, Mutoh T, Chun J (2009) Lysophosphatidic acid (LPA) and its receptors. Curr Opin Pharmacol 9:15-23

Norton WT, Poduslo SE (1973) Myelination in rat brain: method of myelin isolation. J Neurochem 21:749-757

Paxinos G, Franklin KBJ (2001) The mouse brain in stereotaxic coordinates. Academic Press, San Diego

Pedraza C, Sánchez-López J, Castilla-Ortega E, Rosell-Valle C, Zambrana-Infantes E, García-Fernández M, Rodriguez de Fonseca F, Chun J, Santín LJ, Estivill-Torrús G (2013) Fear extinction and acute stress reactivity reveal a role of LPA1 receptor in regulating emotional-like behaviors. Brain Struct Funct. doi: 10.1007/s00429-013-0592-9

Penet MF, Laigle C, Fur YL, Confort-Gouny S, Heurteaux C, Cozzone PJ, Viola A (2006) In vivo characterization of brain morphometric and metabolic endophenotypes in three inbred strains of mice using magnetic resonance techniques. Behav Genet 36:732-744

Peters A, Palay SL, Webster HD (1991) The Fine Structure of the Nervous System: Neurons and Their Supporting Cells. Oxford University Press, New York

Rivers LE, Young KM, Rizzi M, Jamen F, Psachoulia K, Wade A, Kessaris N, Richardson WD (2008) PDGFRA/NG2 glia generate myelinating oligodendrocytes and piriform projection neurons in adult mice. Nat Neurosci 11:1392-1401

Roberts C, Winter P, Shilliam CS, Hughes ZA, Langmead C, Maycox PR, Dawson LA (2005) Neurochemical changes in LPA1 receptor deficient mice-a putative model of schizophrenia. Neurochem Res 30:371-377

Rohrer J, Schweizer A, Russell D, Kornfeld S (1996) The targeting of Lamp1 to lysosomes is dependent on the spacing of its cytoplasmic tail tyrosine sorting motif relative to the membrane. J Cell Biol 132:565-576

Rosenbluth J, Nave KA, Mierzwa A, Schiff R (2006) Subtle myelin defects in PLP-null mice. Glia 54:172-182

Santín L, Bilbao A, Pedraza C, Matas-Rico E, López-Barroso D, Castilla-Ortega E, Sánchez-López J, Riquelme R, Varela-Nieto I, De la Villa P, Suardiaz M, Chun J, Rodríguez de Fonseca F, Estivill-Torrús G (2009) Behavioral phenotype of maLPA1-null mice: increased anxiety-like behavior and spatial memory deficits. Genes Brain Behav 8:772-784

Sherman DL, Brophy PJ (2005) Mechanisms of axon ensheathment and myelin growth. Nat Rev Neurosci 6:683-690

Simone IL, Federico F, Trojano M, Tortorella C, Liguori M, Giannini P, Picciola E, Natile G, Livrea P (1996) High resolution proton MR spectroscopy of cerebrospinal fluid in MS patients. Comparison with biochemical changes in demyelinating plaques. J Neurol Sci 144:182-190

Somogyi P, Takagi H (1982) A note on the use of picric acid-paraformaldehyde-glutaraldehyde fixative for correlated light- and electron microscopic immunocytochemistry. Neuroscience 7:1779

Sohn J, Selvaraj V, Wakayama K, Orosco L, Lee E, Crawford SE, Guo F, Lang J, Horiuchi M, Zarbalis K, Itoh T, Deng W, Pleasure D (2012) PEDF is a novel oligodendrogenic morphogen acting on the adult SVZ and corpus callosum. J Neurosci 32:12152-12164

Sorensen A, Moffat K, Thomson C, Barnett SC (2008) Astrocytes, but not olfactory ensheathing cells or Schwann cells, promote myelination of CNS axons in vitro. Glia 56:750-763

Southwood C, Gow A (2001) Molecular pathways of oligodendrocyte apoptosis revealed by mutations in the proteolipid protein gene. Microsc Res Tech 52:700-708

Southwood CM, Garbern J, Jiang W, Gow A (2002) The unfolded protein response modulates disease severity in Pelizaeus-Merzbacher disease. Neuron 36:585-596

Spohr TC, Choi JW, Gardell SE, Herr DR, Rehen SK, Gomes FC, Chun J (2008) Lysophosphatidic acid receptor-dependent secondary effects via astrocytes promote neuronal differentiation. J Biol Chem 283:7470-7479

Spohr TC, Dezonne RS, Rehen SK, Gomes FC (2011) Astrocytes treated by lysophosphatidic acid induce axonal outgrowth of cortical progenitors through extracellular matrix protein and epidermal growth factor signaling pathway. J Neurochem 119:113-123

Stankoff B, Barron S, Allard J, Barbin G, Noel F, Aigrot MS, Premont J, Sokoloff P, Zalc B, Lubetzki C (2002) Oligodendroglial expression of Edg-2 receptor: developmental analysis and pharmacological responses to lysophosphatidic acid. Mol Cell Neurosci 20:415-428

Steen RG, Ogg RJ (2005) Abnormally high levels of brain N-acetylaspartate in children with sickle cell disease. Am J Neuroradiol 26:463-468

Tigyi G (2010) Aiming drug discovery at lysophosphatidic acid targets. Brit J Pharmacol 161:241-270

Tkachev D, Mimmack ML, Ryan MM, Wayland M, Freeman T, Jones PB, Starkey M, Webster MJ, Yolken RH, Bahn S (2003) Oligodendrocyte dysfunction in schizophrenia and bipolar disorder. Lancet 362:798-804

Trapp BD, Moench M, Pulley E, Barbosa E, Tennekoon GI, Griffin J (1987) Spatial segregation of mRNA encoding myelinspecific proteins. Proc Natl Acad Sci USA 84:7773-7777

Urenjak J, Williams SR, Gadian DG, Noble M (1992) Specific expression of N-acetylaspartate in neurons, oligodendrocyte-type-2 astrocyte progenitors, and immature oligodendrocytes in vitro. J Neurochem 59:55-61

Van der Knaap LJ, van der Ham IJ (2011) How does the corpus callosum mediate interhemispheric transfer? A review. Behav Brain Res 223:211-221

Villarreal G, Hamilton DA, Graham DP, Driscoll I, Qualls C, Petropoulos H, Brooks WM (2004) Reduced area of the corpus callosum in posttraumatic stress disorder. Psychiatry Res 131:227-235

Wang CC (1998) Protein disulfide isomerase assists protein folding as both an isomerase and a chaperone. Ann N Y Acad Sci 864:9-13

Warringa RAJ, Hoeben RC, Koper JW, Sykes JEC, van Golde LMG, Lopes-Cardozo M (1987) Hydrocortisone stimulates the development of oligodendrocytes in primary glial cultures and affects glucose metabolism and lipid synthesis in these cultures. Dev Br Res 34:79-86

Watkins TA, Emery B, Mulinyawe S, Barres BA (2008) Distinct stages of myelination regulated by gamma-secretase and astrocytes in a rapidly myelinating CNS coculture system. Neuron 60:555-569

Weiner JA, Hecht JH, Chun J (1998) Lysophosphatidic acid receptor gene vzg-1/lpA1/edg-2 is expressed by mature oligodendrocytes during myelination in the postnatal murine brain. J Comp Neurol 398:587-598

Werner HB, Kuhlmann K, Shen S, Uecker M, Schardt A, Dimova K, Orfaniotou F, Dhaunchak A, Brinkmann BG, Möbius W, Guarente L, Casaccia-Bonnefil P, Jahn O, Nave KA (2007) Proteolipid protein is required for transport of sirtuin 2 into CNS myelin. J Neurosci 27:7717-7730

West MJ (1993) New stereological methods for counting neurons. Neurobiol Aging 14:275-285

Whitford TJ, Kubicki M, Schneiderman JS, O'Donnell LJ, King R, Alvarado JL, Khan U, Markant D, Nestor PG, Niznikiewicz M, McCarley RW, Westin CF, Shenton ME (2010) Corpus callosum abnormalities and their association with psychotic symptoms in patients with schizophrenia. Biol Psychiatry 68:70-77

Yu N, Lariosa-Willingham KD, Lin FF, Webb M, Rao TS (2004) Characterization of lysophosphatidic acid and sphingosine-1-phosphate-mediated signal transduction in rat cortical oligodendrocytes, Glia 45:17-27

**Figure captions:**

**Figure 1** Reduced myelination in adult $LPA_1$-null mice. **a-f**, Cortical coronal sections from 3-month-old wild-type and ma$LPA_1$-null mice stained with antibodies against myelin proteins MBP (**a-b**), CNPase (**c-d**), and PLP/DM20 (**e-f**). In the absence of the $LPA_1$ receptor, an overall reduction in stained fibers is observed for the three proteins throughout the cortex (ctx, cortical layers indicated by the Roman numerals I through VI) and striatum (st), in which the stained bundle density is similarly affected (insert in **a-b**). Thin sections stained for PLP (**e-f**) demonstrating intense immunoreactivity in the cell soma (arrows) in the null (**f**), compared with the wild-type (**e**) oligodendrocytes. Whereas in the wild-type cells, the label is extended equally in the soma (insert in ***E***, arrow) and cell process (insert in **e**, arrowhead), the null cells demonstrate a strongly labeled PLP in the soma (insert in **f**, arrow). No obvious abnormalities are detected in the corpus callosum (cc) in the null mice, with the exception of the wrinkled appearance of the fibers (asterisk in ***F***, lower panel) compared with fibers in the wild-type mice (**e**, lower panel). Scale bars: **a-f**, ctx, 150 µm; insert in **e** and **f**, 30 µm; **a-f**, st, 75 µm; insert in **a** and **b**, 50 µm; **e** and **f**, cc, 75 µm

**Figure 2** Western-blot analysis of myelin extracts confirming the reduction of myelin proteins in the absence of $LPA_1$. **a**, Representative blots showing the expression of MBP (14, 17, 17.2, 18.5, and 21.5 kDa variants), PLP/DM20, CNPase and GADPH (control) (each indicated by a line) in adult wild-type (wt) and ma$LPA_1$-null (null) myelin extracts from the upper and inner cortical regions containing layers I-III and IV-V, respectively. **b**, Densitometry analysis of band intensities

demonstrating significant reductions (asterisk) in all cortical areas and for the majority of the myelin proteins, in the $LPA_1$-null mice. Data represent the means ± SEM of three independent experiments; n = 8 per group; * $p < 0.05$, Student's t test. O.D., optical density

**Figure 3** MRS in $LPA_1$-null mice demonstrating signs of cell membrane turnover and myelin alterations. **a**, representative MR images of the brain in wild-type (wt) and ma$LPA_1$-null (null) mice showing the voxel locations used in the MRS experiments. **b**, characteristic proton MRS spectra for both genotypes indicating the metabolites N-acetylaspartate (NAA), choline (Cho) and phosphocreatine (Cr) (indicated by arrows). **c**, In vivo spectroscopy areas under NAA and Cho metabolite peaks relative to creatine, i.e., the Cho/Cr and NAA/Cr ratio analyzed at different ages (P30, P60, P110 and P140) demonstrating, in the absence of the $LPA_1$ receptor, a significant increase (asterisk) in the proportion of choline compounds at every age, accompanied with an increase in the NAA levels at the later ages, compared with the wild-type mice. Data are expressed as the mean ± SEM of independent experiments, n = 4 per group; * $p < 0.05$, Student's t test

**Figure 4** The absence of the $LPA_1$ receptor altered myelin compaction, thickness and fiber organization at the ultrastructural level. **a-d**, representative electron micrograph images of the corpus callosum at the level of the fronto-parietal motor cortex in the wild-type and ma$LPA_1$-null brains. The axons in the callosal cross sections in the wild-type mice (**a**) exhibiting a typically compacted myelin sheath; the null corpus callosum (**b**) characterizes by a significant proportion of unmyelinated axons (arrows) and a varying grade of myelin thickness. Longitudinal sections of the corpus callosum demonstrating well-arranged wild-type bundles of fibers (**c**), which is in sharp contrast to the considerable disorganization of the fibers in the absence of the $LPA_1$ receptor (**d**).

**e**, images illustrating the cross sections of the null corpus callosum, showing anomalous irregular morphology and non-compacted myelin and widened extracellular spaces between the lamellae (arrowheads). **f**, micrograph of an oligodendrocyte from the null corpus callosum section exhibiting irregular nuclear morphology and peripherally condensed chromatin. Scale bars: **a-b, f**, 1 µm; **c-d**, 2 µm; **e**, 0.80 µm. **g**, graph shows the percentage of unmyelinated axons in sections from the corpus callosum that are significantly increased (asterisk) in the $LPA_1$-null mice, compared with the wild-type mice. **h**, quantification of the g-ratios in the myelinated axons in the wild-type and null corpus callosum according to axon diameter. The g-ratio was increased significantly in the absence of the $LPA_1$ receptor, confirming the reduction in myelin thickness in the majority of cases. Data for **g-h**, represent the means ± SEM, n = 4 per group; * $p < 0.01$, Student's t test

**Figure 5** Reduced number of differentiating oligodendrocytes in the adult $LPA_1$-null mice. **a**, Immunohistochemistry showing GalC and NG2 expression in cortical (ctx) and striatal (st) sections from adult wild-type and $LPA_1$-null mice. Representative staining is indicated by arrows. The $GalC^+$ cells appear reduced in number throughout the cerebral cortex and in the different layers (left upper panels). Analysis of striatum (left lower panels) demonstrating a similar reduction in the $GalC^+$ cells. In contrast, NG2 immunostaining (right panels) did not demonstrate differences between genotypes. Scale bar, 80 µm. **b-c**, Stereological analysis of the numerical densities demonstrating a significant (asterisk) reduction in $GalC^+$ cells (**b**) in the $LPA_1$-null (null) cortex, compared with the wild-type (wt) cortex, whereas no differences in the $NG2^+$ cells (**c**) were observed. *N*v, cells/$mm^3$; data represent the means ± SEM, n = 6 per group; * $p < 0.05$, ANOVA

**Figure 6** Detectable $LPA_1$-dependent defects in myelination at P30, associated with postnatal myelinating differentiating oligodendroglia. Representative images of cerebral cortex sections from wild-type (**a**) and $LPA_1$-null (**b**) P30 mice, immunostained for MBP and PLP. At P30 and compared with the wild-type mice, the $LPA_1$-null mice exhibited a myelination pattern similar to adult mice, exhibiting a reduction in $MBP^+$ fibers (**a**, **b**, left panels) or PLP/DM20 retention in the cell soma (arrows for comparison) in both the cortex (ctx) and striatum (st) (**a, b**, right panels). ctx, cortical layers indicated by Roman numerals I through VI. Scale bar: left panels, 80 µm; right panels, 40 µm.

**Figure 7** $LPA_1$-dependent defects in myelinating differentiating oligodendroglia not associated with developmental changes. **a-d**, representative images of cerebral cortex sections from wild-type and $LPA_1$-null mice at postnatal age P10, immunostained for MBP, PLP, GalC and NG2. At P10, the mice lacking the $LPA_1$ receptor (**b**) did not display appreciable differences in MBP staining or (remarkably) PLP, which exhibited a cellular location similar to that observed in the wild-type mice (**a**). Similarly, the GalC and NG2 staining did not demonstrate differences between the genotypes at the same age (**c-d**) which was corroborated by the analysis of the respective numerical densities in the cortical P10 mouse samples (**e-f**). ctx, cortical layers indicated by Roman numerals I through VI. Scale bar: 80 µm. *N*v, cells/$mm^3$; Data represent the means ± SEM, n = 6 per group; * $p < 0.05$, ANOVA

**Figure 8** The absence of the $LPA_1$ receptor causes the retention of PLP in the oligodendrocyte soma. **a**, Graphs showing the numerical densities for the $PLP^+$ cells based on the intensity and distribution of the label. The analysis demonstrated a significant (asterisk) reduction in $PLP^+$ cells

in the maLPA$_1$-null mice, which was accompanied by a relevant and significant increase in the proportion of cells exhibiting protein accretion in the soma; the circled diagrams reflect the relative percentages of the differences. Data represent the means ± SEM, n = 6 per group; * $p < 0.05$, ANOVA. **b**, Simple and merged images of double fluorescent immunostaining for PLP (Alexa Fluor® 488) and the RER marker PDI, the Golgi marker Golph4, and the endosomal/lysosomal system marker Lamp1 (Alexa Fluor® 568) in coronal sections from adult wild-type and maLPA$_1$-null mice. In the absence of LPA$_1$ signaling, PLP is retained in the soma colocalizing with PDI, Golph4 (in a number of cells, indicated by arrows), and Lamp1, compared with the wild-type normal oligodendrocytes, in which PLP did not colocalize with any of the markers. Scale bar: 30 µm

**Figure 9** Increased apoptosis in the cortex and corpus callosum of LPA$_1$-null mice. **a-b**, Representative images of the detection of apoptotic cells in brain coronal sections including the cortex (**a**) and corpus callosum (**b**) from adult wild-type and maLPA$_1$-null mice. An increase in apoptotic nuclei was observed in the LPA$_1$-null mice. **c-d**, The estimation of numerical densities for the TUNEL$^+$ cells in the cortical sections (**c**) and quantification of apoptotic nuclei in the corpus callosum sections (**d**) confirmed the histological evidence and demonstrated significantly (asterisk) higher apoptosis in the absence of the LPA$_1$ receptor, compared with the wild-type mice. Scale bar: 30 µm. *N*v, cells/mm$^3$; data represent the means ± SEM, n = 8 per group; * $p < 0.05$, ANOVA and Student's t test

Figure 1
Click here to download high resolution image

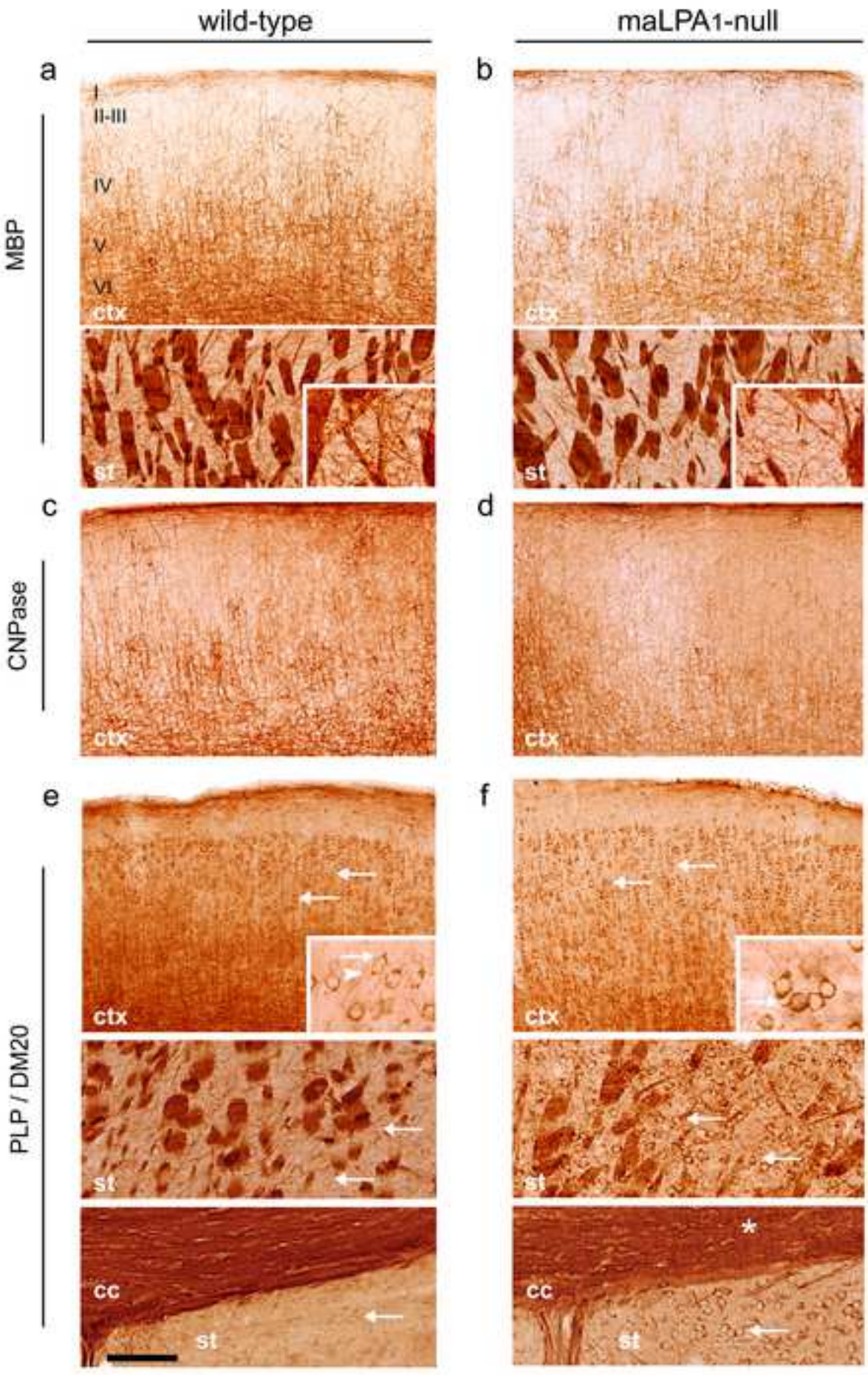

Figure 2
Click here to download high resolution image

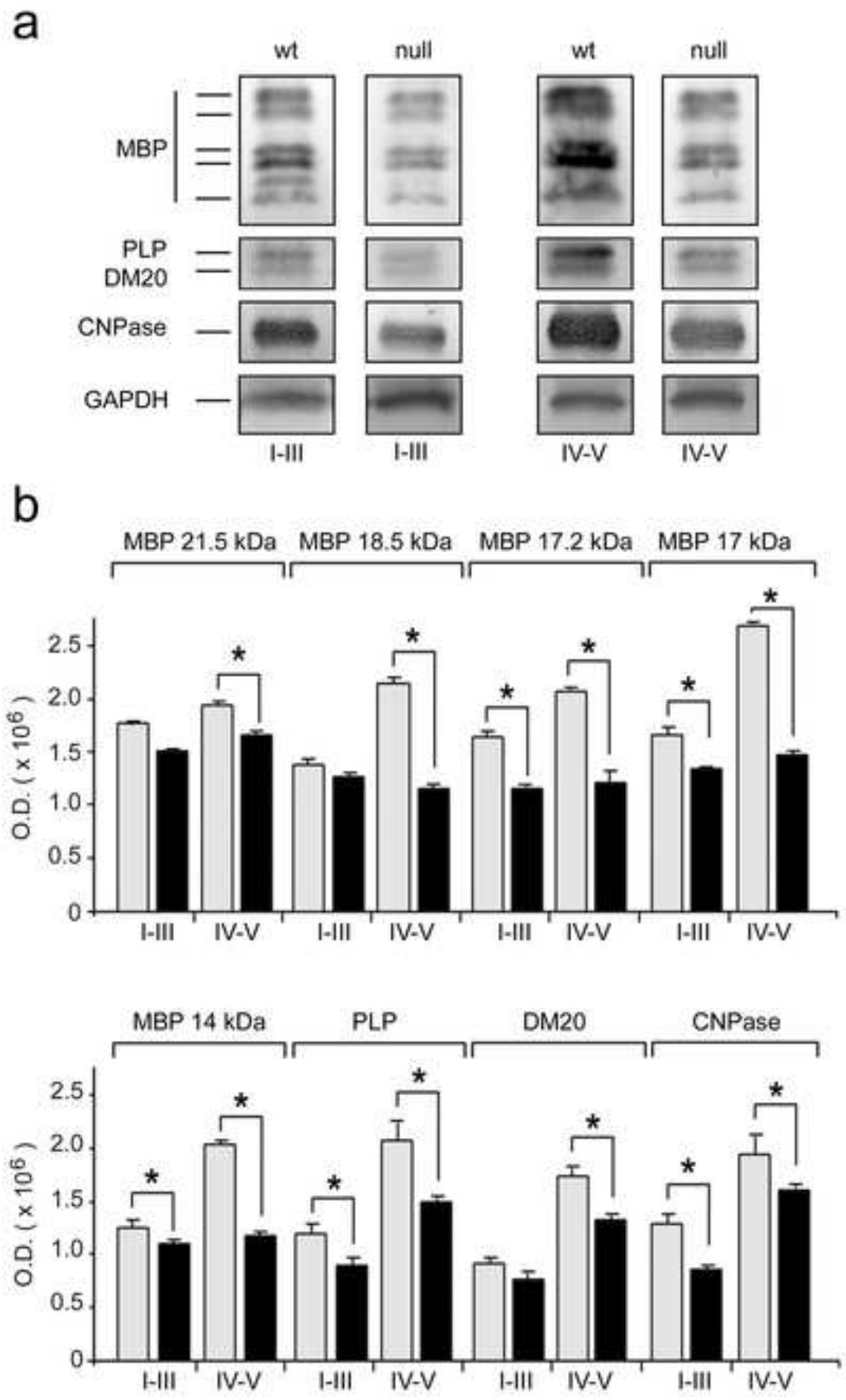

Figure 3
Click here to download high resolution image

a

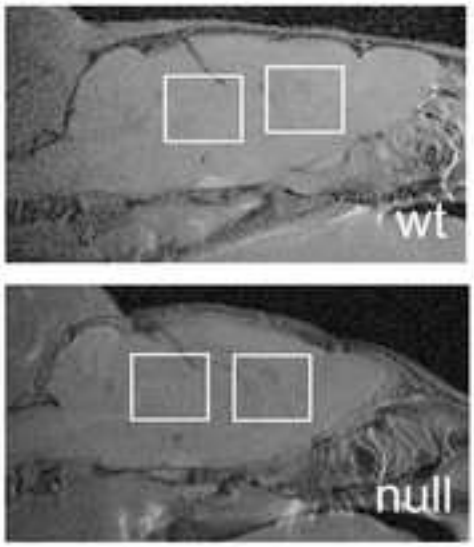


b

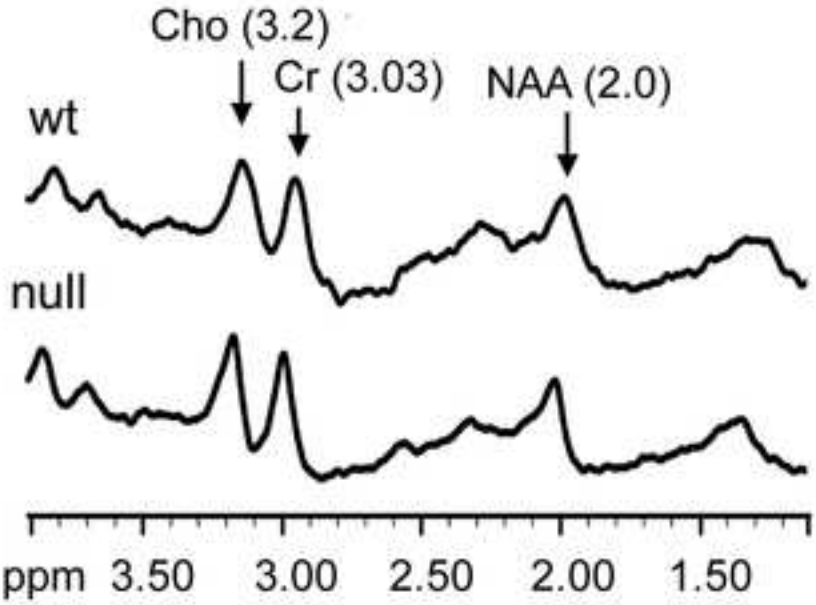


c

| genotype/age | Cho/Cr | NAA/Cr |
|---|---|---|
| wt / P30 | 1.3782 ± 0.0715 | 1.1365 ± 0.0603 |
| null / P30 | 1.5426 ± 0.0823 (*) | 1.2120 ± 0.1355 |
| wt / P60 | 1.4433 ± 0.0354 | 1.1057 ± 0.0296 |
| null / P60 | 1.5618 ± 0.0812 (*) | 1.2362 ± 0.0323 |
| wt / P110 | 1.4006 ± 0.1215 | 1.0546 ± 0.1103 |
| null / P110 | 1.9922 ± 0.3253 (*) | 1.4113 ± 0.1258 (*) |
| wt / P140 | 1.5738 ± 0.0267 | 1.2048 ± 0.0592 |
| null / P140 | 2.0634 ± 0.0496 (*) | 1.6146 ± 0.0506 (*) |

Figure 4

Click here to download high resolution image

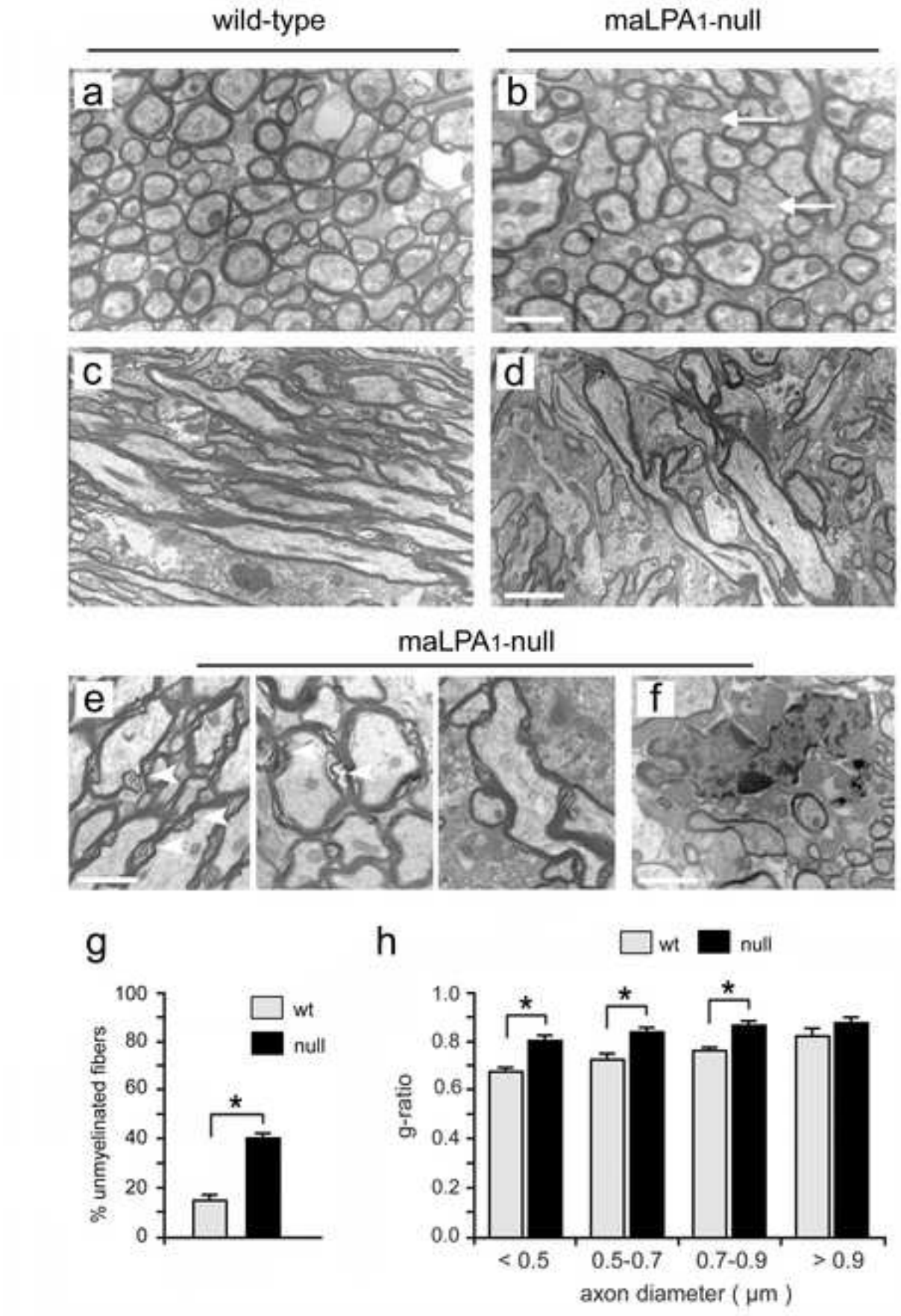

Figure 5
Click here to download high resolution image

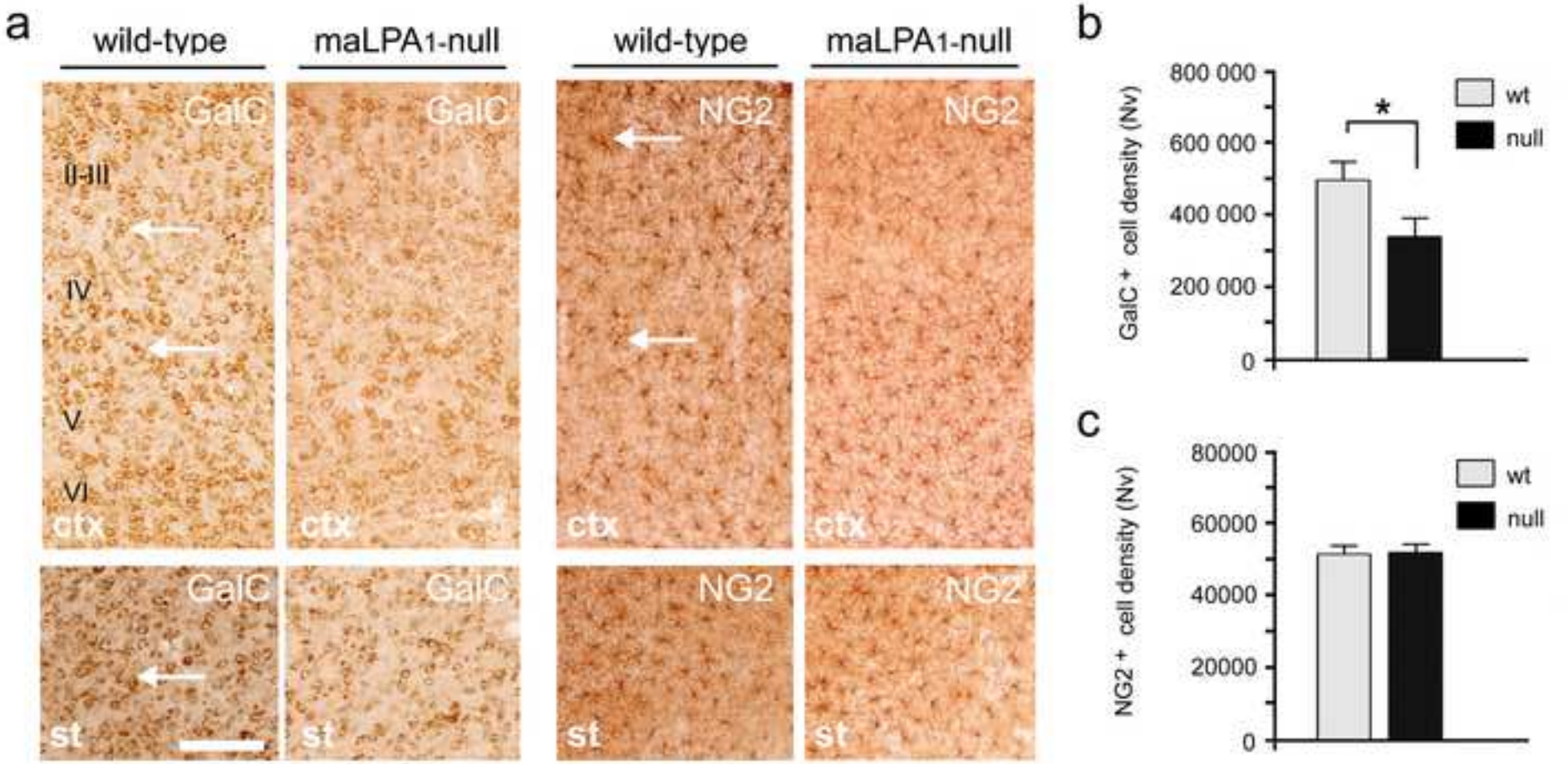

Figure 6
Click here to download high resolution image

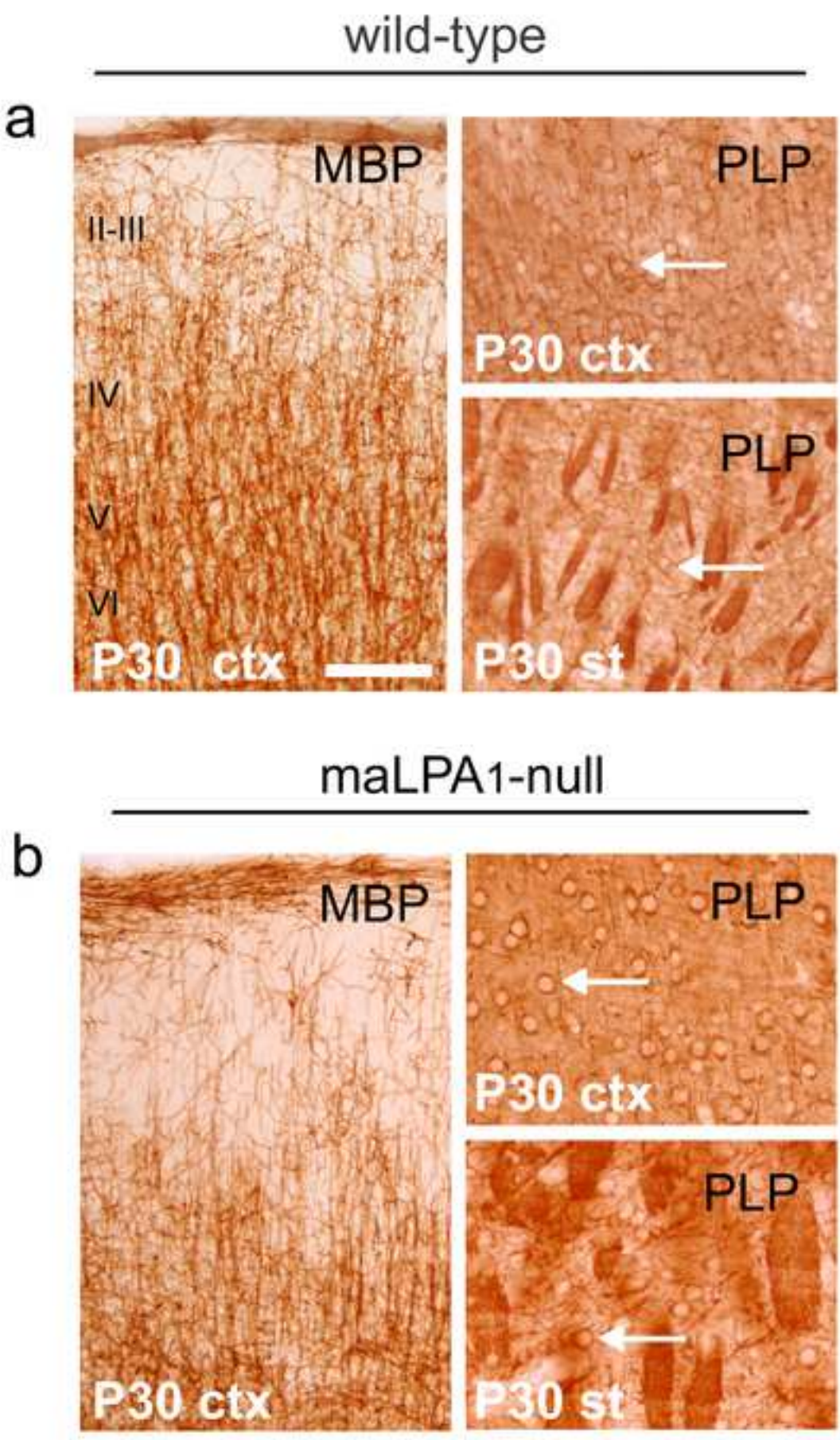

Figure 7
Click here to download high resolution image

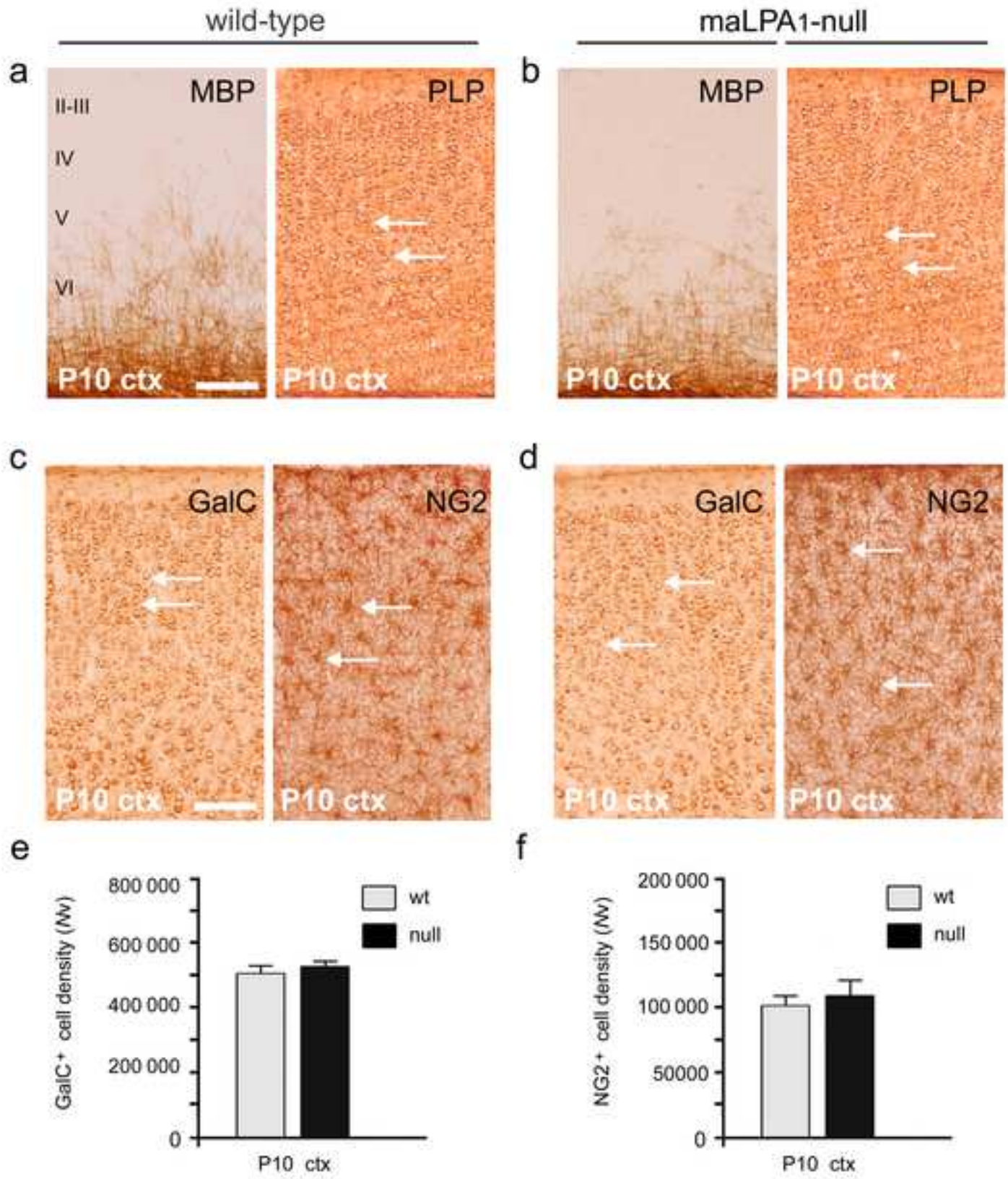

Figure 8
Click here to download high resolution image

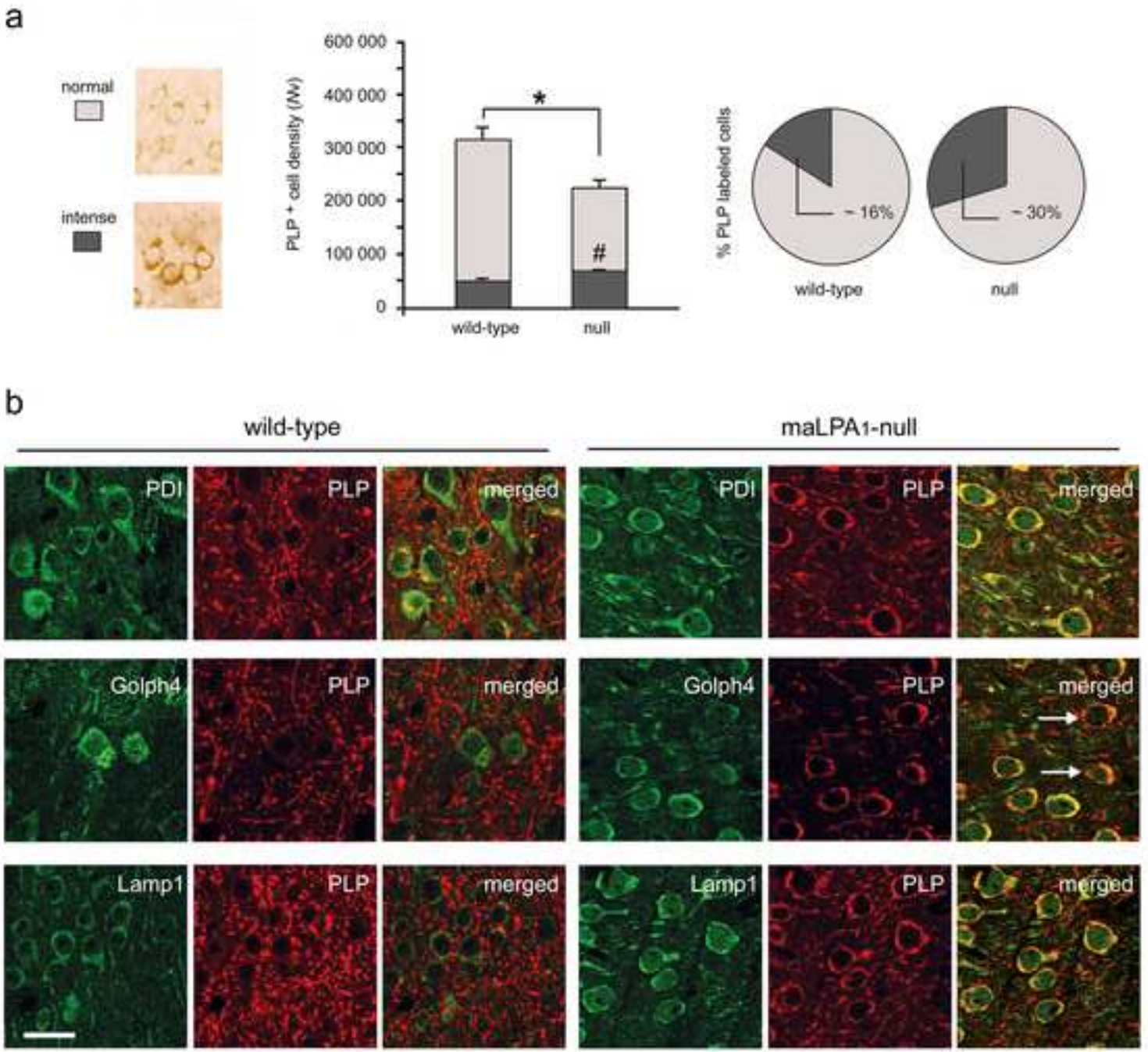

Figure
Click here to download high resolution image

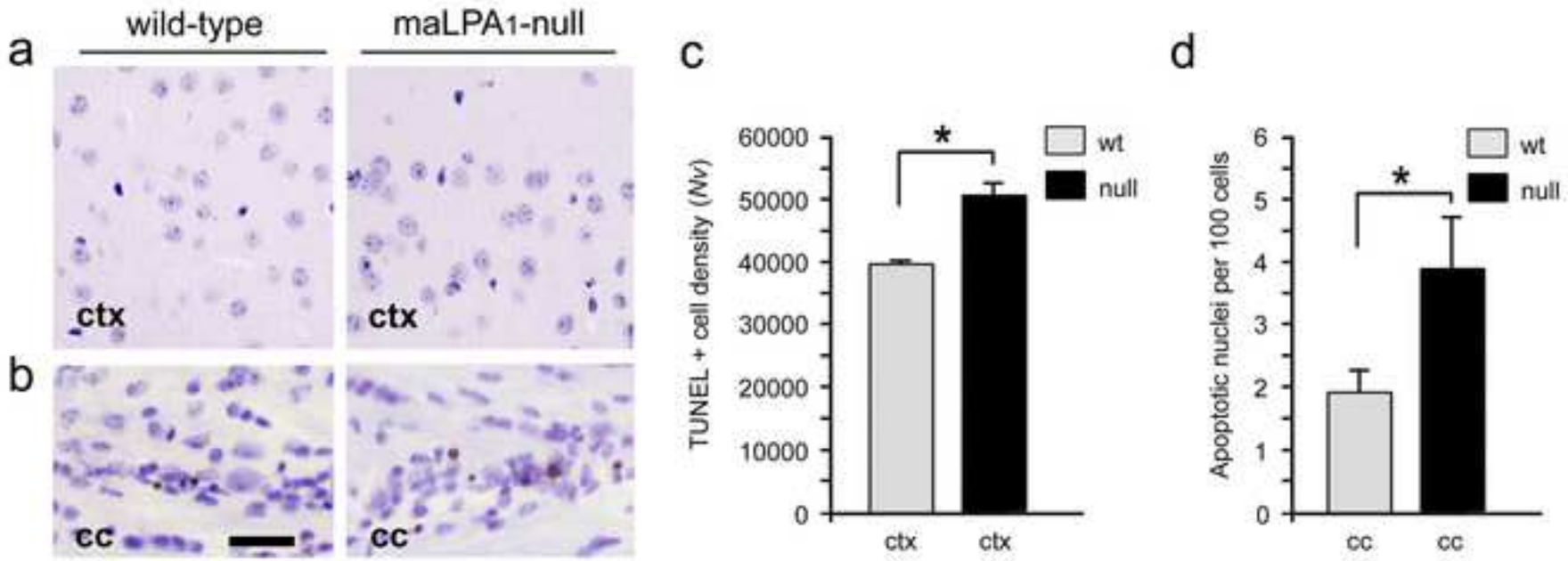

Electronic Supplementary Material
Click here to download Electronic Supplementary Material: renamed_d34c0.pdf

**ELECTRONIC SUPPLEMENTARY MATERIAL**

**Article information and Supplementary Data**

*Title:* **Loss of lysophosphatidic acid receptor $LPA_1$ alters oligodendrocyte differentiation and myelination in the mouse cerebral cortex.**

*Journal name:* **Brain Structure and Function**

*Author names:* Beatriz García-Díaz, Raquel Riquelme, Isabel Varela-Nieto, Antonio Jesús Jiménez, Isabel de Diego, Ana lsabel Gómez-Conde, Elisa Matas-Rico, José Ángel Aguirre, Jerold Chun, Carmen Pedraza, Luis Javier Santín, Oscar Fernández, Fernando Rodríguez de Fonseca , Guillermo Estivill-Torrús.

*Correspondence should be addressed to*: Guillermo Estivill-Torrús; Laboratorio de Investigación y ECAI de Microscopía, UGC Intercentros de Neurociencias, Instituto de Investigación Biomédica de Málaga (IBIMA), Hospitales Universitarios Regional de Málaga y Virgen de la Victoria, Hospital Civil, Pabellón 5, planta sótano, Plaza del Hospital Civil s/n, E-29009, Málaga, Spain; tel: + 34 951290346. e-mail: guillermo.estivill@ibima.eu

**Supplementary Figure 1** $LPA_1$ receptor expression in corpus callosum and cortical white matter fibers. (**a**) In situ hybridization analysis of *Lpar1* expression in brain coronal sections from 3-month-old wild-type (wt) and $maLPA_1$-null (null) mice. Wild-type mice showed strong *Lpar1* expression in the corpus callosum (cc) and stained spread nuclei throughout cortical wall (arrows), in contrast to null mice. (**b**) Brain coronal sections from P30 (postnatal age) wild-type (wt) and null (null) mice immunostained against the $LPA_1$ receptor (left and right panels, respectively), and double immunolabeled against the $LPA_1$ receptor and the Olig2 transcription factor (image at center). In the wild-type cortical sections the $LPA_1$ expression is mainly distributed in the corpus callosum (cc) and cortical white matter fibers delineating the cell processes (arrows) of cells sharing the typical morphology of oligodendrocytes. Null sections are entirely devoid of signal. Double immunolabeling against nuclear transcription factor Olig2 (stained nuclei; arrowheads) and $LPA_1$ (membranous structures; arrows) confirming the oligodendroglial phenotype of $LPA_1$+ cells. cc, corpus callosum; Scale bar: **a**, 200µm; **b**, 100 µm (left, right), 20µm (center)

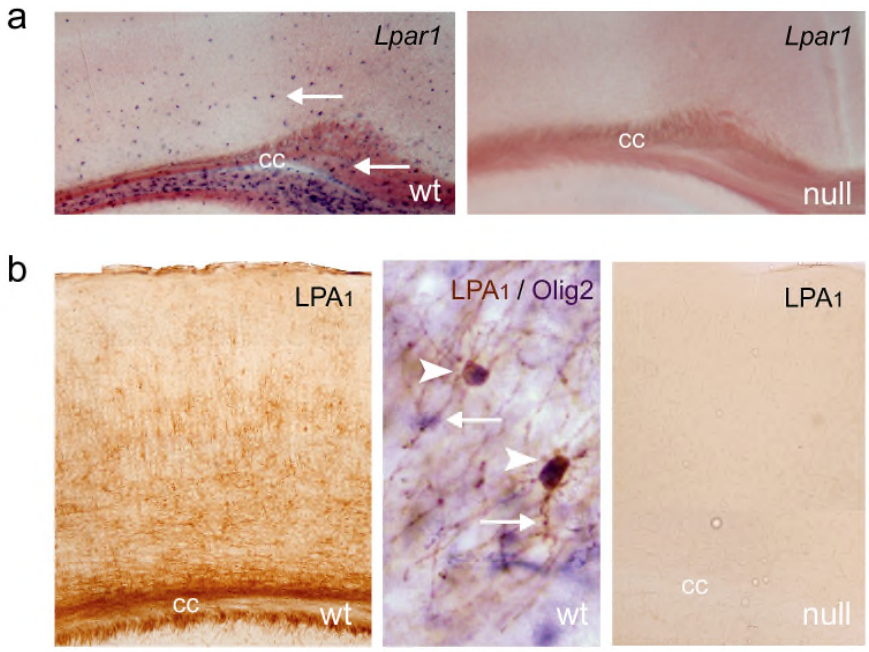

**Supplementary Figure 2** Representative images of brain coronal sections from 3-month-old wild-type (**a)** and maLPA$_1$-null (**b**) mice immunostained for the 200 kD neurofilament protein. The comparative analysis of positive axonal fibers (arrowheads) in somatosensory (left) and motor (right) cortex did not reveal any qualitative evidence for axonal alterations in the absence of the LPA$_1$ receptor. The similar pattern exhibited in both genotypes ruled out the possibility that either the axonal loss or the axonal degeneration could be partially responsible of the myelin defects observed in null cortex. cc, corpus callosum; Scale bar: 100µm

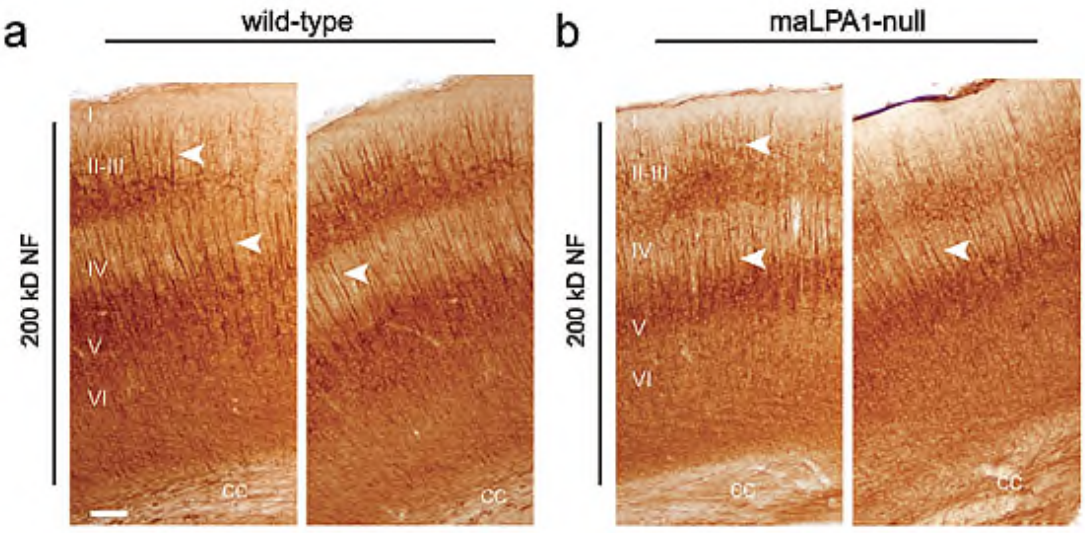

**Supplementary material and methods:**

*In situ hybridization.* In situ hybridization was performed to identify the presence of the *Lpar1* receptor in specific brain areas and cell subtypes. It was performed on adult 3-month-old male mice. At least 4 animals per genotype were used. The mice were transcardially perfused with 0.1 M phosphate-buffered saline (PBS) containing 4 % (w/v) paraformaldehyde. The brains were dissected out into cold phosphate buffer, fixed overnight in the same fixative at 4ºC and kept at same temperature until dehydration in methanol/PBT (phosphate buffered saline, with 0.1% Tween 20). After rehydration, the telencephalon was embedded in a gelatin/ albumin mixture and was cut 200 µm thick sections using a vibroslicer (Campden Instruments). Finally, the sections were dehydrated in methanol/PBT and kept at -20ºC overnight.

In situ hybridization used an *Lpar1* exon3 digoxigenin-labeled riboprobe transcribed from a cDNA plasmid (Contos et al., 1998, 2000). The probes were labeled with digoxigenin-uridine triphosphate (UTP) using commercial kits (Roche Diagnostics; Promega). The hybridization on rehydrated sections was performed at 70ºC, using a water bath, in the presence of formamide. The digoxigenin (DIG)-labeled probe was detected immunocytochemically using an alkaline phosphatase--conjugated digoxigenin antibody (Roche Diagnostics; 1:2000), followed by NBT/BCIP (supplied as a solution of 18.75 mg/ml NBT [Nitro blue tetrazolium chloride] and 9.4 mg/ml BCIP [5-Bromo-4-chloro-3-indolyl phosphate, toluidine salt] in 67% DMSO (v/v); Roche Diagnostics). Finally, the sections were rinsed in PBT overnight at 4ºC, dehydrated and mounted in glycerol/gelatin, and kept at 4ºC until observation.